

ON THE ORIGIN AND EVOLUTION OF WOLF-RAYET CENTRAL STARS OF PLANETARY NEBULAE

By

Kyle David DePew

A THESIS SUBMITTED TO MACQUARIE UNIVERSITY
FOR THE DEGREE OF
DOCTOR OF PHILOSOPHY
DEPARTMENT OF PHYSICS & ASTRONOMY
MARCH 2011



MACQUARIE
UNIVERSITY

FACULTY OF SCIENCE

Except where acknowledged in the customary manner, the material presented in this thesis is, to the best of my knowledge, original and has not been submitted in whole or part for a degree in any university.

Kyle David DePew

Acknowledgements

I must first thank my supervisor, Prof Quentin Parker, for recommending me for the MQRES scholarship and taking me on as his student. I have also benefited enormously from the expertise of A/Prof Orsola De Marco, my co-supervisor, who helped me understand the background of Wolf-Rayet central stars. Special thanks also go to Dr David Frew, who, although not an official supervisor, was just as helpful with his seemingly encyclopedic knowledge of planetary nebulae.

I have been supported by a generous Macquarie University Research Excellence Scholarship during my last three and a half years here. This thesis would not have been possible without significant grants of observing time by the Siding Spring and South African Astronomical Observatory time assignment committees. Thanks also go to all the telescope support staff, especially Donna Burton and Geoff White, for help when everything broke down.

I also thank Madusha Gunawardhana, Quentin Parker and David Frew for graciously allowing me access to their paper on SHS flux calibrations prior to publication.

I would also like to thank my fellow PhD students here in the department. I have been extremely fortunate to work among such thoughtful and enjoyable people. Stacey Bright and Niyas Madapatt especially helped me to remember that there was a world beyond the office and served to distract me (sometimes perhaps too much)

from the tedium of my work. I also thank Anna Kovacevic for training me on the 2.3 Metre Siding Spring Telescope, Korinne McDonnell for LaTeX help and general cubicle mateship, as well as the guys from the quantum information group—Johann-Heinrich Schönfeldt, Gerardo Paz Silva, Aharon Brodutch, Ressa Said, Tommaso De Marie, Mauro Cirio, and all the others—for their camaraderie.

Thanks also go to Duane Hamacher, who first put the idea of moving to Australia into my head, a decision which I have not yet had occasion to regret.

I am also grateful to all the professional staff, especially Carol McNaught, for help with all the paperwork.

Finally, I wish to thank my family, my parents Anne and Ron, my sister Alyssa and brother-in-law Aaron, for never once asking me why I've been studying physics for the past decade plus, and for always understanding my desire to see this through to the bitter end.

List of Publications

Papers and Conference Proceedings Produced in the Course of This Thesis

- **DePew K.**, Parker Q.A., Miszalski B., De Marco O., Frew D.J., Acker A., Kovacevic A.V., Sharp R.G., 2011. *Newly Discovered Wolf-Rayet and Weak Emission-Line Central Stars of Planetary Nebulae*. MNRAS, in press.
- Corradi R.L.M., Valentini M., Munari U., Drew J.E., Rodríguez-Flores E.R., Viironen K., Greimel R., Santander-García M., Sabin L., Mampaso A., Parker Q., **DePew K.**, Sale S.E., Unruh Y.C., Vink J.S., Rodríguez-Gil P., Barlow M.J., Lennon D.J., Groot P.J., Giammanco C., Zijlstra A.A., Walton N.A., 2010. *IPHAS and the symbiotic stars. II. New discoveries and a sample of the most common mimics*. A&A, 509, 41.
- **DePew K.**, Frew D.J., Parker Q.A., De Marco O., 2011. *Wolf-Rayet Central Stars of Planetary Nebulae: Their Evolution and Properties*. APN5 Conf. Proceedings, A.A. Zijlstra, F. Lykou, I. McDonald, E. Lagadec, eds., 160.

Abstract

The origin of hydrogen-deficiency in the central stars of planetary nebulae (CSPNe) is currently a topic of heated debate. This class of objects is comprised of Wolf-Rayet ([WR]) stars, weak emission-line stars (WELS), and PG 1159 stars, each differentiated by a set of unique spectral characteristics. For some time, there have been questions surrounding the evolutionary status of these rare stars: what environmental conditions, such as chemical abundances, are necessary for their emergence, whether any of them represent different stages of development in the same class of stars, and what the characteristics of their progenitors may be. However, such investigations have been hampered by a lack of a sufficient number of these stars and their various sub-classes until recently.

This thesis presents the significant discovery of 22 new [WR] stars and 10 new WELS, many uncovered specifically during this thesis in the course of the MASH survey and through serendipitous fibre placement during follow-up of MASH objects. All examples have been carefully classified as accurately as possible using the best current available data though for many this remains a preliminary assignment pending deeper spectra. This work expands the known sample of H-deficient stars by 30%, allowing a more detailed study of their properties than previously possible and moving us closer to a more complete census of local H-deficient CSPNe.

In the course of our classifications, Abell 48 was found to be a particularly interesting object. Further analysis of nebular chemical abundances, modeled temperature, and ionization state as indicated by the chemical species present suggests that the CSPN of Abell 48 may be very similar to the CSPN of PB 8, which has recently been redesignated as the founding member of a new and rare [WN/WC] class (Todt et al. 2010). Its similarity to and differences with other oxygen-rich [WO] and carbon-rich [WC] stars as well as previously identified [WN] stars are examined.

All these stars have also been studied in the context of a new subclass-dynamical age relationship that we have also discovered. This major finding is the first to show evidence of an evolutionary trend amongst the [WR] population and was made possible by use of the powerful new surface brightness-radius (SB-r) relation of Frew (2008) that can, at last, provide accurate distances to PN (and hence also their central stars). Key data acquired here as well as modeled effective temperatures and excitation classes of other [WR]s, WELS and PG 1159 central stars found in the literature were also utilized in generating this relationship.

Finally, continuing with the SB-r relation, the scale heights of the most complete available sample of [WR], WELS and PG 1159 CS populations are determined and compared. These data show that both WELS and PG 1159 stars are found to possess significantly higher Galactic heights than the members of the [WR] class, implying that PG 1159s do not all descend from [WR]s, and that WELS are not evolutionarily related to [WR]s. This is another major finding of this work. It is possible, however, that the WELS class, and perhaps the PG 1159 class as well, are heterogeneous groups.

Contents

Acknowledgements	v
List of Publications	vii
Abstract	ix
List of Figures	xvii
List of Tables	xxix
1 Introduction	1
1.1 Life Cycle of Low- to Intermediate-Mass Stars	2
1.1.1 Introduction to the Hertzsprung-Russell Diagram	3
1.1.2 Description of the Life Cycle of Low- to Intermediate-Mass Stars	3
1.1.3 Description of PNe	6
1.2 Past PNe Surveys	9
1.3 Central stars of PNe	11
1.4 General Spectral Classifications of Massive Wolf-Rayet Stars	12
1.4.1 General Properties of Massive Wolf-Rayet Stars	15
1.4.2 Theorized Evolution of Massive Wolf-Rayet Stars	16

1.5	Wolf-Rayet Central Stars of PNe and their classification	22
1.6	Taxonomy of Hydrogen-Deficient Central Stars of PNe	25
1.6.1	Theorized Evolution of Wolf-Rayet Central Stars of PNe and Thermal Pulse Scenarios	27
1.6.2	The Born Again Scenario	30
1.6.3	PG 1159 and WELS Stars	31
1.6.4	Modeling of [WR] Stars	35
1.7	Conclusion	36
2	Data Reduction	37
2.1	The Dual Beam Spectrograph	38
2.2	Basic Spectroscopic Data Required	39
2.2.1	Bias Frames	40
2.2.2	Dark Frames	41
2.2.3	Flat-Field Frames	41
2.2.4	Sky Flats	41
2.2.5	Calibration Frames	42
2.2.6	Target frames	42
2.2.7	Cosmic Rays	42
2.2.8	Spectrophotometric Standard Stars	42
2.3	Spectroscopic Data Acquired During This Thesis	43
2.4	The Image Reduction and Analysis Facility; IRAF	43
2.4.1	Reduction of DBS Data	44
2.4.2	Flat Preparation	45
2.4.3	Flat Subtraction	47
2.4.4	Cosmic Ray Cleaning	48
2.4.5	Spectrum Extraction	48
2.4.6	Wavelength Calibration	50

2.4.7	Flux Calibration	51
2.5	WiFeS Data	52
2.5.1	File Preparation	53
2.5.2	Calibrations	54
2.5.3	Final Reduction	55
2.6	SPIRAL Data Reduction	55
2.6.1	Data Preparation	56
2.6.2	Data Reduction	60
3	New and Old Hydrogen-Deficient Objects	63
3.1	Introduction	64
3.1.1	[WR]s in the MASH Sample	67
3.2	Spectroscopic Observations	68
3.3	Classification Schemes	71
3.4	Individual Objects	72
3.4.1	New [WR] Stars	75
3.4.2	Possible [WR]s and WELS	84
3.5	Conclusions	89
3.6	Comprehensive Table of Hydrogen-Deficient Central Stars of Planetary Nebulae	89
4	Abell 48 and the [WN/WC] Class	105
4.1	Introduction	106
4.2	Massive WR stars and the WN Class	107
4.3	The Putative [WN] Class	107
4.3.1	PM5	108
4.3.2	LMC-N66	109
4.3.3	PB8	112

4.3.4	Considerations for [WN] Stars	112
4.4	Spectroscopic Observations	114
4.5	Flux Measurements and Distance Calculation	115
4.6	Reddening	116
4.6.1	Abell 48: Planetary Nebula or Massive Ring Nebula?	117
4.7	The Abell 48 Nebula–Spectral Characteristics and Other Properties	119
4.8	The Central Star	121
4.8.1	Central Star Properties	124
4.9	Nebular Plasma Diagnostics and Line Ratios	127
4.9.1	Electron Temperature	129
4.9.2	Electron Density	129
4.9.3	Finding Plasma Diagnostics and Abundances Using HOPPLA	130
4.10	Calculating the Ionized Mass	136
4.11	Comparison with PB 8	138
4.12	Evolutionary Considerations	139
4.12.1	The AGB Final Thermal Pulse	141
4.12.2	The Late Thermal Pulse	141
4.12.3	The Very Late Thermal Pulse	142
4.12.4	Which Pathway for Abell 48?	142
4.13	Conclusions	143
5	New Evolutionary Relationships for Wolf-Rayet Central Stars of Planetary Nebulae	147
5.1	Introduction	148
5.2	The H α Surface Brightness-Radius Relationship	149
5.3	Determination of Planetary Nebula Dynamical Age	155
5.4	The [WR] Dynamical Age Sequence	156
5.5	Excitation Classes and Effective Temperatures	157

5.5.1	Constructing an Excitation Class- [WR] Subclass Function . . .	160
5.6	H α Surface Brightness Evolution	163
5.7	Discussion & Conclusions	168
6	A Comparison of the Galactic [WR], WELS and PG 1159 CSPN Populations	171
6.1	Introduction	172
6.2	Data Collection and Analysis	173
6.3	Galactic Distributions	173
6.3.1	Considerations Involving White Dwarfs	187
6.4	Evolutionary Scenarios	189
6.5	Conclusions	190
7	Conclusions	199
7.1	The [WR] Population	200
7.2	The [WN/WC] Stars	200
7.3	The Subclass Evolutionary Sequence	202
7.4	The Evolutionary Relationship Between [WR]s, WELS and PG1159 Stars	202
7.5	Future Work	203
	References	205

List of Figures

1.1	An example of a Hertzsprung-Russell diagram showing the evolution of a $2 M_{\odot}$ star of solar metallicity. Note the main sequence line in the right lower quadrant. The blue line represents a born-again track, triggered by a very late thermal pulse (see §1.6.2). The red star represents PG 1159-035, an H-deficient star, and the green star represents NGC 6853, an H-normal star. Numerical labels indicate the logarithm of the approximate time in years for the indicated evolutionary phase. Taken from Herwig (2005).	4
1.2	A diagram of the layers of an AGB star. During the AGB phase, a star will begin thermal pulsations. Convection currents will form in the convective zone, eventually throwing core matter into the surrounding space and enriching it with nucleosynthetic elements. Adapted from Karakas et al. (2002).	5
1.3	The Wolf-Rayet spectral classifications of van der Hucht (2001). This system was developed for use with massive Wolf-Rayets.	13
1.4	The WR classification system of Crowther et al. (1998). This system was developed for both massive and CSPN types of Wolf-Rayets.	14

-
- 1.5 An example of a Wolf-Rayet spectrum, from star WR1, the first Wolf-Rayet star identified. Note the strong emission lines. Retrieved from <http://www.amateurspectroscopy.com/Astrophysics-spectrum.htm> on 6 March 2008. 16
- 1.6 Spectra of several [WR] stars, taken from Parker & Morgan (2003). . . 24
- 1.7 This figure, from Acker & Neiner (2003), shows the drastic difference in linewidth between several [WO4]pec stars and a WELS star. The thick line gives the spectrum for M 1-51, the thin solid line Cn 1-5, M 1-32 the dashed line, and PM 1-89 the dashed-dotted line. The dotted line shows the spectrum of M 1-61, a WELS star, for contrast. 32
- 2.1 A picture of the DBS, mounted on the 2.3 Metre telescope. The blue arm is to the left and the red is to the right. 39
- 2.2 Example frames taken on the 2.3m in May 2008. At top is a bias frame. The noisy nature is apparent. The middle frame is a flat-field taken with a quartz lamp. The illumination is smooth, as the lamp emits a continuum of wavelengths. This is in contrast to the example arc lamp exposure at bottom, which clearly shows the distinct wavelengths produced in the gas. 40
- 2.3 A simplified flow chart illustrating the basic data reduction process. As illustrated, dark frames (if necessary) are subtracted from a target frame, while the bias signal of the chip is subtracted off of the flat-field image. The quotient of the remaining science image and the perfect flat is taken to produce the output image, which will then be wavelength- and flux-calibrated. 45

2.4	An image of the CCD chip after observing the planetary nebula Abell 48 through the blue arm of the 2.3 Metre Dual Beam Spectrograph. The spatial direction (the direction of the slit) is along the vertical axis, and the dispersion direction is along the horizontal axis. This observation was taken 11 May 2008.	47
2.5	An image of the CCD chip after observing the planetary nebula Abell 48 through the red arm of the 2.3 Metre Dual Beam Spectrograph (DBS). As before, the spatial direction is along the vertical axis, and the dispersion direction is along the horizontal axis. This exposure was taken concurrently with the blue image on 11 May 2008.	47
2.6	The previously presented spectrum after cosmic ray cleaning.	49
2.7	A screenshot of PNDR. The horizontal lines represent the upper and lower bounds of regions on the plate which the user wishes to be binned. Separate regions are designated for sky (background) lines, for upper and lower nebular regions (either side of the star), and the star itself.	50
2.8	An example of a nebular spectrum awaiting wavelength- and flux-calibration.	51
2.9	The selection of gratings available on WiFeS. Taken from the the Australian National University WiFeS user pages (http://msowww.anu.edu.au/observing/ssowiki/index.php/WiFeS_Main_Page).	53
2.10	The image slicer of WiFeS, as shown in the observing manual, available at http://msowww.anu.edu.au/observing/ssowiki/index.php/WiFeS_Main_Page . Note the concentric design, which follows the same concepts as McGregor et al. (1999) and McGregor et al. (2003).	53
2.11	An image of the PN PB8 in H α after subtracting sky lines.	55
2.12	The AAOmega spectrograph.	56
2.13	A schematic diagram of AAOmega, showing the red camera in high dispersion mode, and the blue camera in low dispersion mode.	57

2.14	The SPIRAL IFU, which is designed for use with AAOmega. Its 32×16 array of fibres allows a possible 512 separate spectra.	57
2.15	At left is a composite colour image of the MASH PN PHR1811-3042 (see Chapter 3) with $H\alpha$, short red and B band images represented as red, green and blue respectively, obtained from the online SuperCOSMOS survey data (Parker et al. 2005). At right is the same PN observed by SPIRAL at commissioning on 28 June 2006. Images taken from Sharp & The Aaomega+Spiral Team (2006a).	58
2.16	The 2dfdr data reduction facility interface.	59
3.1	A montage of the new MASH [WR] and WELS PNe, ordered according to Galactic longitude. Each $H\alpha$ /SR/ B_J composite colour image is accompanied by the $H\alpha$ /short-red quotient image to its right. The $H\alpha$ /SR images are from the SuperCOSMOS $H\alpha$ Survey (Parker et al. 2005) and the B_J images from Hambly et al. (2001). The lengths of the image sides in arcseconds are presented alongside the name of each object. North is to the top and east is to the left for all images.	73
3.2	A montage of the non-MASH PNe found to contain a true or candidate [WR] or WELS central star. As in Fig. 3.4, each $H\alpha$ /SR/ B_J composite colour image (Parker et al. 2005; Hambly et al. 2001) is accompanied by the $H\alpha$ /short-red quotient image to its right. Again, the lengths of the image sides in arcseconds are presented alongside the name of each object. North is to the top and east is to the left for all images.	74
3.3	Spectra of objects whose central stars have recently been identified as being [WR]s or WELS; all spectra have been rectified. The most prominent lines have been identified (dashed lines and labels).	90

3.4	Spectra of objects whose central stars have recently been identified as being [WR]s or WELS; all spectra have been rectified. The most prominent lines have been identified (dashed lines and labels).	91
3.5	Spectra of objects whose central stars have recently been identified as being [WR]s or WELS; all spectra have been rectified. The most prominent lines have been identified (dashed lines and labels).	92
3.6	Spectra of objects whose central stars have recently been identified as being [WR]s or WELS; all spectra have been rectified. The most prominent lines have been identified (dashed lines and labels).	93
4.1	The spectrum of LMC-N66 as observed in 1995 and 1996, as presented in Peña et al. (1997a). The upper two cover the UV and blue range, and the bottom two expand the spectral regions around the He II, C IV and N V lines to show the substructure evident in these features.	110
4.2	The best fitting model of PB 8's spectrum, adapted from Todt et al. (2010).	113
4.3	A montage of all currently known [WN] and [WN/WC] objects. Clockwise from top left are Abell 48, PB8, LMC-N66, and PM5. Abell 48, PB8 and PM5 are shown in $H\alpha$ /SR/ B_J false-colour composites where $H\alpha$ is represented by red, SR by green, and B_J by blue (Parker et al. 2005). All apart from LMC-N66 are $60'' \times 60''$. $5'' \times 5''$ HST STIS image of LMC-N66, taken from Peña et al. (2004), was observed through the MIRVIS grating. Note the bipolar appearance of LMC-N66 and PB8 compared to the spherical and elliptical appearances of PM5 and Abell 48, respectively, showing that there do not appear to be any common morphological traits in the surrounding nebulae.	118

4.4	The spectrum of PM 5, as presented in Morgan et al. (2003). Note the 7118Å feature, which may be mistaken for a broad C II line, but derives instead from a series of N IV lines.	119
4.5	The SHASSA image of Abell 48. The coarse resolution (48" pixels) reduces this PN to four pixels, designated by the concentric circles. . .	120
4.6	Three images of Abell 48. At left, a false-colour image of Abell 48 in the J, H and K bands from 2MASS (Skrutskie et al. 2006). J, H and K wavelengths are represented as blue, green and red respectively. Image dimensions are 3" × 3". The faint purple extended ring of emission is expected from a true PN (Cohen et al. 2010). At middle is a composite H α /SR/B $_J$ colour image (Parker et al. 2005), and at right is a radio image of Abell 48 from NVSS (Condon & Kaplan 1998). Dimensions in the middle and right panels are 90" × 90".	121
4.7	The blue nebular spectra of Abell 48 and PB 8 for comparison, obtained from WiFeS, with the three important nebular lines—H β λ 4861 and [O III] $\lambda\lambda$ 4959,5007 labelled.	122
4.8	The red nebular spectra of Abell 48 and PB 8 for comparison, obtained from WiFeS, with labelled nebular lines at [O I] λ 6300, [N II] $\lambda\lambda$ 6548,84, H α λ 6563 and [S II] $\lambda\lambda$ 6717,31.	123
4.9	A close-up view of the [S II] lines at 6717 and 6731Å, normally used for plasma diagnostics.	124
4.10	The blue spectrum of the central star of Abell 48, taken by Wachter et al. on 4 Sep 2008 with the 200" Hale Telescope at Palomar Observatory. The spectral resolution is approximately 5-7 Å. Note the presence of N V $\lambda\lambda$ 4604,4620 and the prominent He II λ 4686 feature.	127

-
- 4.11 The red spectrum of the central star of Abell 48. Again, this spectrum was taken by Wachter et al. on 4 Sep 2008 with the 200" Hale Telescope at Palomar Observatory. The spectral resolution is approximately 5-7 Å. Note the He II λ 5412 line and the N IV λ 7116 feature, which can be mistaken for a C II λ 7118 line. 128
- 4.12 The dereddened spectral energy distribution of the central star of Abell 48, reconstructed from photometric measurements from the available literature sources. The points represent the dereddened fluxes of the central star. Massive WN overlays have been divided by constant factors to match the magnitude in V in order to compare slopes. Note the very close fit by the 50.1 kK model. Massive WN models courtesy of Jim Herald. 134
- 4.13 An H α image divided by the broad-band 'SR' quotient image of Abell 48, created using SHS data. There appear to be two sets of faint arcs that might be associated with previous ejecta from the host star that are identified here for the first time. To the northwest there appear to be two faint closely spaced arcs about 30 arcseconds in extent, with the outermost being 46 arcseconds from the CSPN. To the south there appears to be another faint shorter arc some 105 arcseconds from the CSPN. These could be evidence for opposing jets ejected prior to the main nebular shell, as seen in other PNe such as NGC 3918. The different observed angular distances of the northern and southern arcs from the CSPN could be the result of their projection onto the plane of the sky rather than anything dynamical. 140

-
- 4.14 A $5'' \times 5''$ $H\alpha$ image divided by broad-band 'SR' quotient image of PB8 created using SHS data. There is a faint outer asymmetric shell outside of the inner nebula (centered on the host star) that is clearly associated. Again this represents previous ejecta from the host star that has been identified here for the first time. The northeast section of the shell is $38''$ from the CSPN and the southwest component $27''$ from the CSPN. The fact that the only two known [WN/WC] CSs reside in PNe that possess faint outer haloes may be significant if it reflects some ejection mechanism related to the star's chemistry. 145
- 5.1 The surface brightness-log radius (SB-r) relation, based on a sample of 122 calibrating PNe. The line is a least-squares bisector fit (Isobe et al. 1990). Taken from Frew (2008). 151
- 5.2 A comparison of high-excitation (HE) and common-envelope PNe together versus others, illustrating the systematically lower $H\alpha$ surface brightnesses in the former group. Taken from Frew (2008). 152
- 5.3 The subclass-dynamical age relationship. Subclass index indicates: [WO1]=1, . . . , [WO4]=4, [WC4]=5, . . . , [WC11]=12. WELS are represented by subclass index 13 and PG1159 stars are represented at number 0. PB 8 has been placed at subclass index 6.5, consistent with its former classification of [WC5-6] (Acker & Neiner 2003). Note the apparent quick evolution from [WC9] to [WC5]. 157
- 5.4 The subclass-excitation class relationship, using the ρ EC method of Reid & Parker (2010). As above, subclass index indicates: [WO1]=1, . . . , [WO4]=4, [WC4]=5, . . . , [WC11]=12. A distinct general trend is clearly evident with the hottest CSPN inferred from the high excitation class values correlating with the early [WO] subclass. 161

5.5	The subclass-effective temperature relationship. 'X's represent [WR]s, stars the WELS, squares the [WC]-PG1159s, and triangles the [WN/WC] stars PB 8 and Abell 48. The WELS denoted by half-filled pentagons represent upper limits for the central stars of NGC 6543 and NGC 6629. Temperature sources are noted in Table 5.3.	166
5.6	H α surface brightness versus spectral type of H-deficient CSPNe.	167
6.1	The Galactic distribution of the [WR], WELS and PG 1159 stars in our sample. The figure is oriented such that an observer looking toward the centre of the Galaxy finds objects with small positive longitudinal values on the left, positive Galactic latitude direction up, etc.	175
6.2	A histogram showing the distribution of [WR]s as a function of Galactic height $ z $. The black line corresponds to the exponential fit function.	176
6.3	A histogram showing the distribution of WELS as a function of Galactic height $ z $	176
6.4	A histogram showing the distribution of PG 1159 central stars as a function of Galactic height $ z $	177
6.5	The distribution of [WR], WELS and PG 1159 stars with derived distances smaller than 3 kpc, where the significant differences between the [WR], WELS and PG 1159 Galactic height distributions can be seen more clearly.	182
6.6	A histogram showing the distribution of a volume-limited sample of [WR] central stars as a function of Galactic height $ z $. Here all included [WR]s are within 3 kpc. Note that 26 of the 28 [WR]s in this sample have $ z $ heights below 300 pc.	183
6.7	A histogram showing the distribution of a volume-limited sample of WELS central stars as a function of Galactic height $ z $. Here all WELS within 3 kpc are included in the plot.	184

-
- 6.8 The changing spectrum of Longmore 4, as presented in Werner et al. (1992). Note the sudden appearance and gradual decline of emission lines C IV $\lambda 4658$ and He II $\lambda 4686$, to the point where they form an absorption trough in the last spectrum, consistent with a PG 1159 star. C IV $\lambda\lambda 5801,12$, O IV $\lambda\lambda 5279,5289$ and He II $\lambda 6560$ also briefly appear before declining in strength. 186
- 6.9 A plot of calculated PG 1159 PN radii versus effective temperatures. There does not seem to be a relationship between the two variables. . . 187
- 6.10 One possible evolution scenario for the evolution of [WR]s, in which the [WCL]s evolve into [WCE]s, [WO]s, down through the PG 1159 stages and into the white dwarf region of the H-R diagram. Boxes are overlaid on top of the H-R diagram of Herwig (2005). 190
- 6.11 A second possible evolution scenario for the evolution of [WR]s, in which the [WCL]s evolve into WELS before becoming [WCE]s. This possibility is considered because WELS effective temperatures and H α surface brightnesses fall between those of [WCL]s and [WCE]s. This scenario is however unlikely because of the difference in Galactic heights between these populations. 191
- 6.12 A third possible evolution scenario for the evolution of [WR]s, in which the PG 1159 class is a common endpoint for both [WR] and H-deficient WELS evolution. 192
- 6.13 A possible evolution scenario for the evolution of WELS, in which the H-rich types evolve into hybrid PG 1159 and then DAO and DA white dwarfs. 193
- 6.14 The typical evolution sequence for aging H-rich central stars, for comparison. 194

6.15	The spectrum of the binary central star V477 Lyrae, presented in Pol- lacco & Bell (1994). Note the N III-C III-C IV $\lambda 4650$ complex.	196
6.16	Two WELS spectra from Marcolino & de Araújo (2003). Note the sim- ilarity of the N III-C III-C IV $\lambda 4650$ complex to that seen in Figure 6.15.	197

List of Tables

2.1	A summary of observing runs carried out in the course of this thesis. Spectral resolution and wavelength coverage varied according to the specific gratings used on the night. Please refer to later chapters for details on these values.	44
3.1	Observational details of the new CSPNe discovery spectra.	70
3.2	A list of the newly discovered [WR] CSPNe, along with WELS found in the course of examining the sample. The top portion lists all of those PNe from the MASH sample, while those objects below the line are for previously known PNe.	88
3.3	All known Galactic PNe with [WR], WELS and PG1159 central stars. .	94
3.4	All known Galactic PNe with [WR], WELS and PG1159 central stars. .	95
3.5	All known Galactic PNe with [WR], WELS and PG1159 central stars. .	96
3.6	All known Galactic PNe with [WR], WELS and PG1159 central stars. .	97
3.7	All known Galactic PNe with [WR], WELS and PG1159 central stars. .	98
3.8	All known Galactic PNe with [WR], WELS and PG1159 central stars. .	99
3.9	Observation details of the objects listed in Appendix A.	102

3.10	Below are FWHM, EW and dereddened intensities of stellar lines in our discovery spectra. The FWHM and EW of C IV $\lambda\lambda 5801,12$ and C III $\lambda 5696$ are marked. All other columns are the intensities of the lines, with C IV $\lambda\lambda 5801,12 = 100$. (We do not list the absolute C IV line fluxes because our spectra were not absolutely flux calibrated.) Spaces marked ‘-’ were not seen in the spectra. ‘N.O.’ indicates that the designated line lay in a region of the spectrum which was not observed. ‘P’ indicates that the line is present, but the exact value cannot be measured due to the absence of the continuum or C IV $\lambda\lambda 5801,12$. ‘S’ indicates a strong line. ‘W’ signifies a weak line. Again, ‘:’ denotes an uncertain value, while ‘::’ indicates a very uncertain value.	104
4.1	Properties of the [WN/WC] Stars	113
4.2	Observation details for Abell 48. All observations were taken at Siding Spring Observatory, on the 2.3 metre telescope, using the Wide Field Spectrograph (WiFeS).	114
4.3	An abbreviated comparison of quantities for Abell 48 if it is a PN versus a ring nebula.	118
4.4	Nebular lines found in Abell 48, taken from the 2.3 metre April 2010 spectrum. $\lambda_{Helio}(\text{\AA})$ signifies the wavelength after heliocentric correction. The flux of H β is in 10^{-15} erg/cm ² /s/ \AA , but the remainder are set such that H β =100.	132
4.5	Stellar lines found in the CSPN of Abell 48, taken from the spectra of Wachter et al. (2010) and our own WiFeS data. λ_{Helio} represents the heliocentric velocity corrected wavelength of the line, while λ_{Sys} signifies the wavelength after systemic velocity correction. λ_{Lab} denotes the laboratory measured value.	133
4.6	Photometric values of the central stars of Abell 48 and PB 8.	135

4.7	Nebular chemical abundances, obtained from HOPPLA. Here $\log(H) = 12$. Line ratios for the PB 8 analysis were taken from Girard et al. (2007). Abundances for Abell 48 are only lower limits (see §4.11).	138
4.8	Properties of the central stars of Abell 48 and PB 8. Values for PB 8 have been taken from Todt et al. (2010).	139
5.1	Wolf-Rayet, WELS and PG 1159 central stars used for the subclass-dynamical age relation.	158
5.2	Wolf-Rayet central stars used for the subclass-excitation class relation, with relative intensities and excitation classes.	162
5.3	Wolf-Rayet central stars used for the subclass-temperature relation.	164
5.4	H-deficient central stars used for the subclass- $H\alpha$ surface brightness relation.	165
5.5	H-deficient central stars used for the subclass- $H\alpha$ surface brightness relation (continued).	167
6.1	The numbers of known [WR], WELS and PG 1159 star CSPNe, before and after MASH, as well as the number that are known to be within 3 kpc, and the average Galactic height $ z $ and scale heights. It must be noted that the number within 3 kpc is merely a lower limit.	173
6.2	Galactic Distribution of Objects	178
6.3	Galactic Distribution of Objects	179
6.4	Galactic Distribution of Objects	180

1

Introduction

*In the beginning the Universe was created. This has made a lot of people
very angry and has been widely regarded as a bad move.*

–Douglas Adams, *The Restaurant at the End of the Universe*

Overview

This thesis concerns Wolf-Rayet central stars of planetary nebulae (PNe hereafter). These objects, while rare (only around 100 are known at present), constitute a very important and dynamic part of the Galactic stellar population. Given their unique

properties, these central stars are important tests of our theories of stellar evolution. Their chemistries and evolutionary paths are still subjects of intense study.

The following sections serve to introduce PNe in general, with a focus on those PNe with Wolf-Rayet central stars (denoted [WR] hereafter), on which this thesis is based. It will also summarize past surveys of nebulae and theory surrounding the evolution of Wolf-Rayets, including the massive types, which are evolutionarily unrelated but which display very similar spectral properties and with which they can be confused. Specifically, this thesis aims to: (i) introduce a significant number of new [WR]s discovered during spectroscopic follow-up of PN candidates uncovered by the Macquarie/AAO/Strasbourg H α PN surveys (MASH: Parker et al. 2006, Miszalski et al. 2008), (ii) examine the case for the existence of a rare, new [WN/WC] star, the central star of Abell 48, that we have uncovered, only the second known member of this putative class, (iii) to construct a new subclass-dynamical age relationship to test existing theories of [WR] evolution, and (iv) investigate the Galactic distribution, including scale height, of [WR]s and weak emission-line stars (WELS) to determine whether or not they are related. Points (iii) and (iv) in particular have only become possible through the concurrent development by members of our MASH team of a powerful new distance technique that can be applied to the PNe surrounding these objects.

With these overall objectives in mind, we begin with a discussion of the stellar life cycles of low- to intermediate-mass stars.

1.1 Life Cycle of Low- to Intermediate-Mass Stars

Stars undergo many changes during their lifetimes. While PNe represent the final stages of the average (i.e. low- to intermediate-mass: $M_{\star} \sim 0.8\text{-}8$ solar masses or M_{\odot}) star's life, it is necessary to discuss the events which lead to this state in order to

understand the composition and properties of old stars.

1.1.1 Introduction to the Hertzsprung-Russell Diagram

The characteristics of stars are primarily defined by their temperatures and luminosities, or rates of energy production. For this reason, astronomers employ a graph called the Hertzsprung-Russell diagram, which plots these two quantities against each other. Temperature is usually represented as decreasing from left to right, while luminosity increases from bottom to top. An H-R diagram is widely used to show the evolution of a star, as its temperature and luminosity change throughout its lifetime. See Figure 1.1.

1.1.2 Description of the Life Cycle of Low- to Intermediate-Mass Stars

A star arises by gravitational accretion of matter in a proto-stellar cloud of gas and dust. Low- to intermediate-mass stars then migrate to, and live out the majority of their lives on, the main sequence, which is represented by a line moving roughly from the upper left hand corner to the lower right. Initial position on the main sequence is determined by initial mass.

Stars found along this track are still in the process of fusing hydrogen into helium in their cores. When the hydrogen in the core is exhausted and insufficient radiation pressure is being exerted by the core on the outer shells of the star, the star will begin to contract, thereby heating the helium in the core and igniting hydrogen fusion in a shell above. This process drastically increases the radiation pressure again, to the point that the outer envelope of the star expands to a hundred times its original radius or more.

As the gas in the outer envelope expands and cools, the star becomes a red giant.

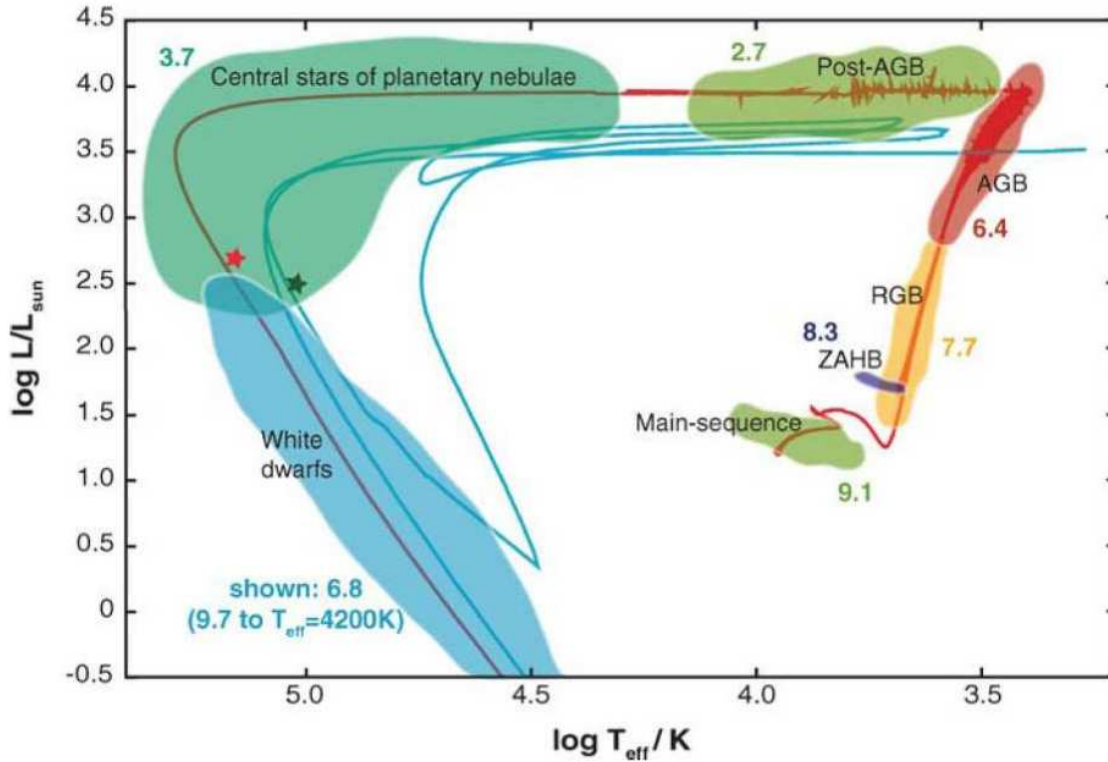


FIGURE 1.1: An example of a Hertzsprung-Russell diagram showing the evolution of a $2 M_{\odot}$ star of solar metallicity. Note the main sequence line in the right lower quadrant. The blue line represents a born-again track, triggered by a very late thermal pulse (see §1.6.2). The red star represents PG 1159-035, an H-deficient star, and the green star represents NGC 6853, an H-normal star. Numerical labels indicate the logarithm of the approximate time in years for the indicated evolutionary phase. Taken from Herwig (2005).

During the hydrogen shell burning, helium ash will fall onto the core, further increasing its mass and the pressure on it.

The star, after some mass loss driven by stellar winds, will contract again after core He-ignition. (If the star has a mass $M \lesssim 2.3 M_{\odot}$, this time it will overcome electron degeneracy pressure, igniting the core in what is referred to as the helium flash.) At this point, the star enters onto what is called the *horizontal branch*, so called for the appearance of such evolved stars across this location on the H-R diagram. During

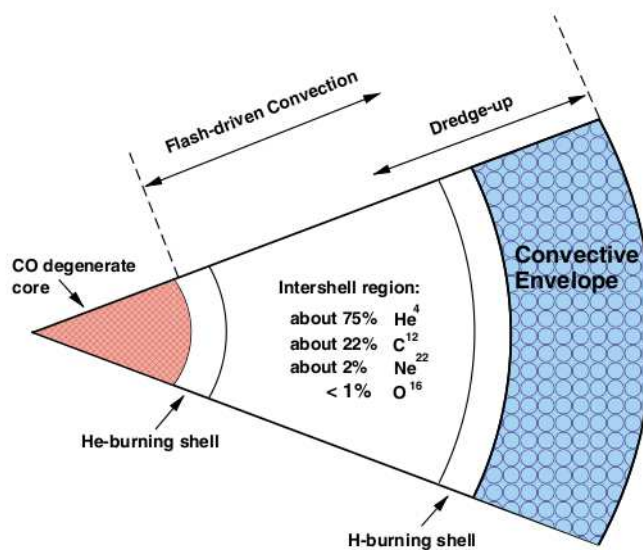


FIGURE 1.2: A diagram of the layers of an AGB star. During the AGB phase, a star will begin thermal pulsations. Convection currents will form in the convective zone, eventually throwing core matter into the surrounding space and enriching it with nucleosynthetic elements. Adapted from Karakas et al. (2002).

this stage, helium burning causes the core to expand and thus decreases the rate of energy production. The star will then contract and heat up again. When all the helium in the core has been fused into carbon and oxygen through the triple- α process, the star contracts again, igniting new helium- and hydrogen-burning shells. At the end of this phase, the star undergoes thermal pulsations and core matter dredge-up, expelling enriched matter into the surrounding area as it traverses the *asymptotic giant branch* (AGB) of the H-R diagram. As more and more matter is thrown off, ever hotter regions of the star are exposed until sufficient ultraviolet radiation emerges to ionize the surrounding previously ejected gas, at which point the circumstellar cloud has become a detectable PN. Central stars of PNe are therefore, as a rule, very hot, blue stars which are on their way to becoming white dwarfs.

1.1.3 Description of PNe

PNe constitute an important stage in the late life cycle of stars and the associated processing of enriched stellar matter in the cosmos. This period follows the AGB phase which is characterized by high mass loss from the parent star and the cessation of thermal pulses and dredge-up. This process is necessary for the redistribution of processed elements (particularly carbon and nitrogen) into the interstellar medium (ISM).

However, PNe constitute a very short period in the life of a star, usually on the order of only several tens of thousands of years (Zijlstra & Pottasch 1991), compared to the several billion spent on the main sequence. This is because PNe quickly become too faint to observe, as the glowing, gaseous envelopes have an expansion rate which, although modest ($\sim 25 \text{ km s}^{-1}$), eventually rarefies the gas while the shell itself is subjected to an increasingly diluted radiation field as time passes. While young PNe might have densities on the order of $\sim 10^6$ particles per cm^3 , older specimens generally exhibit values in the range of 10^2 - 10^4 particles per cm^3 . At the same time, the stellar nucleus shrinks to a radius many times smaller than its original size on its way to becoming a white dwarf with a radius similar to that of our own planet, dramatically decreasing the luminosity of the star. Magnitudes of the nuclei can easily drop from $M_V = -3$ to $+5$. For this reason, it is often necessary to probe for the [O III] $\lambda 5007$ signature of these objects, since a significant percentage (up to $\sim 10\%$; Ciardullo et al. 2005) of their energy is emitted in this line and, in the absence of significant dust and extinction, is often the strongest emission line seen in their visible spectra.

Classification of PNe by Type

Planetary nebulae have been generally classified into five basic types though a wide variety of classification schemes published in the literature. Note that in this classification scheme described below, the underlying nature of the PN and its Galactic context

are addressed rather than their projected angular appearance, which is the basis for the wide variety of morphological classification schemes. The first four types were suggested by Peimbert (1978), and a fifth was defined later by Faundez-Abans & Maciel (1987).

Type I is a class reserved for helium- and nitrogen-rich PNe, and arise from intermediate-mass progenitors ($>3\text{-}4 M_{\odot}$; Sterling & Dinerstein 2008). Their N/O ratio is at least 0.8 (Kingsburgh & Barlow 1994). Type I central stars of planetary nebulae (CSPNe) belong to Population I, the most metal-rich class of stars (as opposed to Population II stars, which are older and have lower metallicities) and most of them are found to be bipolar (Peimbert 1978; Peimbert & Torres-Peimbert 1983). As a class, they tend to have larger than average diameters and expansion velocities (Corradi & Schwarz 1995), hotter and more massive central stars (Tylenda 1989), smaller scale heights (e.g. Stanghellini 2000), and deviate from the circular rotation of the Galaxy. A significant portion (a bit less than 20%) of the ~ 1500 newly discovered MASH PNe belong to this type, owing to the survey's low latitude coverage (Parker et al. 2006). (The MASH survey will be discussed later.)

Type II is an intermediate class that corresponds to progenitors of roughly $M = 1.5 M_{\odot}$. These nebulae have nearly circular orbits around the Galaxy and therefore have Galactocentric distances very similar to that of their birthplace. Older members of this group will have traveled farther due to their longer evolution time. Most PNe are Type II. Maciel (1989) split this type into two subtypes: Type IIa, or Population I Type II nebulae, and Type IIb, or Population II Type II nebulae.

Type III PNe, or “high velocity” PNe, are defined as those PNe which possess a peculiar radial velocity greater than 60 km s^{-1} and do not belong to the halo population. These PNe form from disk population stars.

Type IV is comprised of the halo population of PNe. This is currently a very small group. At the time of Peimbert's initial classification, only three such nebulae

were known to him. Only about a dozen are now identified as such (Perinotto 2007). Type IV nebulae do not show excesses of helium, and actually seem to exhibit less of this element when compared to other PNe. It is thought that in these objects, most of the hydrogen-rich envelope is ejected to form the PN shell. It is believed that Type I PNe correspond to the most massive progenitors, while Type IV PNe correspond to the least massive.

PNe are also grouped according to three general morphological classes: spherical, bipolar, and elliptical nebulae. Bipolar nebulae are generally larger and more massive at a given surface brightness (Frew et al. 2006). This type is thought to comprise about one-fifth of all PNe, both WR and non-WR (Parker et al. 2006). They seem to descend from higher-mass progenitor stars (greater than 2 solar masses; Peimbert & Serrano 1980; Phillips 2001). Bipolar PNe also have higher than average expansion velocities and diameters, as well as hotter and more massive central stars (Tylenda & Stasińska 1989). They also show strongly enhanced nitrogen, helium and neon abundances (e.g. Corradi & Schwarz 1995) and exhibit molecular H₂ emission (Zuckerman & Gatley 1988; Kastner et al. 1996). They are generally restricted to lower average galactic latitudes and scale heights (Parker et al. 2006; Corradi & Schwarz 1995).

Excitation Classes assigned to PNe

The excitation class is a quantity that essentially measures the helium excitation of a nebula and it is intended as a proxy for the effective temperature of the central star. It was first defined by Aller (1956) building on the work of Page (1942), but has since undergone several “revisions”. Feast (1968) and Webster (1975) both formulated their own classification criteria based on the original Aller equations. These in turn served as the basis for Morgan (1984), who devised a system for the Magellanic Cloud PNe. Dopita & Meatheringham (1990), dissatisfied with the stepwise classification system, decided to create a new one which was based on continuous functions. Dopita and

Meatheringham defined the excitation class ρ such that:

$$\rho = 0.45 \left(\frac{F([\text{OIII}] 5007\text{\AA})}{F(H\beta 4861\text{\AA})} \right), 0 < \rho < 5 \quad (1.1)$$

and

$$\rho = 5.54 \left(\frac{F(\text{HeII } 4686\text{\AA})}{F(H\beta 4861\text{\AA})} + 0.78 \right), 5 \leq \rho < 10 \quad (1.2)$$

Note that this definition does not completely do away with a step-wise function; Dopita & Meatheringham still found it necessary to use a discontinuous, two-piece equation.

More recently a new excitation class definition has been introduced by Reid & Parker (2010) which has been shown to exhibit a much closer correlation with the best available Zanstra temperature estimates than all other schemes. Excitation class has also been studied with respect to other variables, such as expansion velocity (e.g. Medina & Peña 2002). These studies will be discussed later.

1.2 Past PNe Surveys

Several surveys have been conducted to search for PNe, and the most significant early examples by Kohoutek and Acker have been extensively summarized in other papers (e.g. Parker et al. 1999). More recent PNe surveys have utilized narrow-band $H\alpha$ imaging to find candidates (e.g. Rodgers et al. 1960; Kogure et al. 1982). However, these surveys were, for the most part, accomplished photographically on Schmidt-type telescopes to get wide field coverage. As a result, they suffered from low resolution and sensitivity but did uncover new PNe. For example, Davies et al. (1976) used a fast but coarse-grained 098-04 emulsion which resulted in relatively poor resolution. Others in the late 1990s (e.g. Russeil 1997; Russeil et al. 1998) employed more modern detectors, but, with their more limited fields-of-view, concentrated on small regions for in-depth

study. Still other researchers have sacrificed spatial resolution for wide area coverage and good velocity resolution (e.g. Reynolds et al. 1998) which is useful for untangling large-scale gaseous kinematics but is of very limited utility for uncovering, small new PNe.

Following these early efforts, several astronomers have focused on specific frequency bands in order to enhance our understanding of the individual processes that go on in PNe. Cohen (1999) completed mid-infrared studies, Martin (1999) infrared, while radio observations were made by English et al. (1998), Green (1999) and Higgs (1999). Molecular line studies have also been performed by Oliver et al. (1996) and Heyer (1999). Later, the SuperCOSMOS H α Survey (SHS; Parker et al. 2005) and the Macquarie/AAO/Strasbourg H α PNe project (MASH; Parker et al. 2006) were commissioned in order to better map the gaseous emission component of the Southern Milky Way and to specifically trawl for new PNe and then follow-up the discovered candidates spectroscopically. The SHS was unique in that it combined good sensitivity, wide field coverage and resolution on the order of an arcsecond (Parker et al. 1999). The first new PNe discoveries of the MASH survey came out of direct visual scrutiny of the original SHS films on a light table with a microscope. By 2003, the survey films had been digitised by the SuperCOSMOS microdensitometer at the Royal Observatory Edinburgh and the SHS then became available online. This permitted more sophisticated and automated searches for previously missed PNe. These formed the basis for the MASH-II PN survey (Miszalski et al. 2008).

The MASH survey has been very successful, increasing the number of known PNe by almost 1300, an increase of roughly 80% (Parker et al. 2006). Interestingly, it has also reclassified eleven objects that were previously designated as galaxies as bona-fide PNe based on follow-up spectroscopy. Although charge coupled devices (CCDs) are predominantly used now in professional astronomy for imaging, the original H α survey on which the MASH discoveries were based employed fine-grained Kodak Technical

Pan film (Parker & Malin 1999), and as a result yielded a high degree of detail. The film has a sensitivity peak near the frequency of $H\alpha$ and, when prepared properly, allows high resolution (320 lines/mm) and detector quantum efficiency ($\sim 10\%$), the best possible for photographic film (Phillipps & Parker 1993). In order to distinguish between stellar lines and lines from the nebula, a spectral resolution of at least 5000 is generally necessary (Medina et al. 2006).

As the survey was done using the United Kingdom Schmidt Telescope (UKST), MASH contains only PNe which are visible from the southern hemisphere. Because of the sensitivity of the film, many of the newly discovered PNe are rather faint and old, and some could only be detected in $H\alpha$. As a result, much more can be learned as to the later evolution of these objects. Prior to MASH, roughly a third of all known PNe were catalogued as point sources (Parker et al. 1999), indicating the skew of data toward young, high luminosity objects. Fainter PNe are generally more evolved and extended. The central stars have also faded, meaning that the morphological features of the matter in the nebula are more visible. This may also enable better abundance determinations for the central stars due to the rarefaction of the nebula in the line of sight to the star.

1.3 Central stars of PNe

The central stars of PNe form a very heterogeneous group and have been quite difficult to identify unequivocally for many PNe because they are often very faint in the optical. This lack of homogeneity amongst their observed properties has been one of the main reasons why they cannot be used in any distance determination technique that relies on a specific well-behaved property, such as that exhibited by Cepheids. Currently only about 20% of PNe have central stars which have been classified. While being generally blue photometrically, because of their necessarily high temperatures, they exhibit a

wide range of spectral properties. There is among these a specific class of PN central stars that exhibit strong, broad emission lines across much of the optical spectrum, which gives them unusual colours. These broad lines indicate fast winds of up to several thousand km s^{-1} and high mass loss rates ($\gtrsim 10^{-6} M_{\odot}$). In fact their observed spectral features bear an uncanny resemblance to the well-known massive Population I stars classified as Wolf-Rayet (WR) stars. In this case, stars of different initial masses and evolutionary states can nevertheless give rise to the same basic observable phenomena. Both kinds of star can also possess surrounding nebulae so it is also not always clear-cut what kind of central object is giving rise to the observed spectrum. Clearly it is important to be able to distinguish those central stars of PNe from their massive counterparts which may (or may not) lack a surrounding nebula. In the literature, PNe with central stars exhibiting Wolf-Rayet features are usually designated as [WR]. The square brackets distinguish them from their massive counterparts. However, the first archetypal Wolf-Rayet stars identified belonged to the massive star variety, and they have certain unique features and stellar evolution sequences. For this reason, an explanation of WR stars in general is necessary.

1.4 General Spectral Classifications of Massive Wolf-Rayet Stars

The first three WR stars were discovered in the constellation Cygnus by Charles Wolf and Georges Rayet at the Paris Observatory, all within one degree of one another, and were subsequently described in a paper (Wolf & Rayet 1867) as exhibiting unusually strong and broad emission lines. The cause of their unique spectra was not immediately understood, though. It was not until Gamow (1943) that the broad emission lines were first suggested to be the result of nuclear processed material on their surfaces. However, this was not universally established until late in the twentieth century (Lamers et al.

1991).

Wolf-Rayets have been divided into three primary classifications of WN, WO and WC stars, depending on the predominance of nitrogen, oxygen or carbon respectively in their spectra, and furthermore into “early” and “late” types in the case of WC and WN stars. See Tables 1.3 and 1.4 for the essential discriminatory criteria of two classification systems. While van der Hucht (2001) uses a fairly straightforward, one- or two-criteria classification system, Crowther et al. (1998) employ a scheme that specifies the FWHM and ratios for certain spectral line intensities observed. However, the FWHM is used more as a “guideline”, and not so much as an actual criterion of the respective class.

WN types	Nitrogen emission lines	Other emission criteria
WN2	N v weak or absent	He II strong
WN2.5	N v present, N IV absent	
WN3	N IV \ll N v, N III weak or absent	
WN4	N IV \approx N v, N III weak or absent	
WN4.5	N IV $>$ N v, N III weak or absent	
WN5	N III \approx N IV \approx N v	
WN6	N III \approx N IV, N v present but weak	
WN7	N III $>$ N IV, N III $<$ He II 4686	He I weak P-Cyg
WN8	N III \gg N IV, N III \approx He II 4686	He I strong P-Cyg
WN9	N III $>$ N II, N IV absent	He I P-Cyg
WN10	N III \approx N II	Balmer lines, He I P-Cyg
WN11	N II \approx He II, N III weak or absent	Balmer lines, He I P-Cyg
WC types	Carbon emission lines	Other emission criteria
WC4	C IV strong, C II weak or absent	O v moderate
WC5	C III \ll C IV	C III $<$ O v
WC6	C III \ll C IV	C III $>$ O v
WC7	C III $<$ C IV	C III \gg O v
WC8	C III $>$ C IV	C II absent, O v weak or absent
WC9	C III $>$ C IV	C II present, O v weak or absent
WO types	Oxygen emission lines	Other emission criteria
WO1	O VII \geq O v, O VIII present	C III absent
WO2	O VII $<$ O v	C IV $<$ O VI, C III absent
WO3	O VII weak or absent	C IV \approx O VI, C III absent
WO4		C IV \gg O VI, C III absent

FIGURE 1.3: The Wolf-Rayet spectral classifications of van der Hucht (2001). This system was developed for use with massive Wolf-Rayets.

WO stars are generally classed from WO1 to WO4, but no higher, so that all WO stars are labelled as “early” types. Early types tend to have higher ionization levels and angular sizes amongst their surrounding nebula, and are hotter and less luminous than the “late” types.

WN and WC stars exhibit the products of the CNO cycle (H-burning) and the

Subtype	FWHM (\AA)	Primary	Secondary	Additional Criteria	Examples	
		C III $\lambda 5696$	C IV $\lambda 5808$ /C III $\lambda 5696$	C IV $\lambda 5808$ /C II $\lambda 4267$	He II $\lambda 4686$ /He I $\lambda 5876$	
		$\log W_\lambda$ or $\log I_\lambda$	$\log W_\lambda$	$\log W_\lambda$		
WC11	~ 3	≤ -1.2	≤ -1.5	He II $\lambda 4686$ absent	K2-16	
WC10	3-6	-1.2 to -0.7	-1.5 to -0.2	≤ -0.8	CPD-56 ^o 8032	
WC9	30 \pm 15	-0.7 to -0.3	-0.2 to +1.0	-0.8 to +0.1	He 2-99, HD 164270	
WC8	40 \pm 10	-0.3 to +0.1	≥ 1.0	≥ 0.1	HD 192103, NGC40	
		C IV $\lambda 5808$	C III $\lambda 5696$ /O III-v $\lambda 5590$	O VI $\lambda 3818$ /C IV $\lambda 5808$		
		$\log W_\lambda$ or $\log I_\lambda$	$\log W_\lambda$ or $\log I_\lambda$	$\log W_\lambda$		
WC7	45 \pm 20	+0.1 to +0.6	≥ 0.1	≤ -1.5	HD 156327	
WC6	50 \pm 20	+0.6 to +1.1	+0.0 to +0.7	≤ -1.5	HD 92806	
WC5	50 \pm 20	+1.1 to +1.5	-0.4 to +0.5	≤ -1.5	HD 165763, M1-25	
WC4	70 \pm 20	≥ 1.5	≤ -0.4	≤ -1.5	HD 32257, NGC 5315	
		C IV $\lambda 5808$	O VI $\lambda 3818$ /O V $\lambda 5590$	O VI $\lambda 3818$ /C IV $\lambda 5808$	O VII $\lambda 5670$ /O V $\lambda 5590$	
		$\log W_\lambda$	$\log W_\lambda$	$\log W_\lambda$		
WO4	60 \pm 30	-0.3 to +0.25	-1.5 to -1	$\ll 0.0$	MS4, NGC1501	
WO3	90 \pm 30	+0.25 to +0.6	-1 to +0.2	$\ll 0.0$	Sand 2, NGC7026	
WO2	160 \pm 20	+0.6 to +1.1	$\geq +0.2$	≤ 0.0	Sand 4	
WO1	40 \pm 10	≥ 1.1	$\geq +0.2$	≥ 0.0	NGC 6905	

FIGURE 1.4: The WR classification system of Crowther et al. (1998). This system was developed for both massive and CSPN types of Wolf-Rayets.

triple- α process (He-burning) respectively. WN stars also exhibit emission lines that are much less prominent than those of WC stars (Massey 2003). In late WN (WNL) stars, nitrogen dominates over carbon. These objects are the most massive WR stars (usually in excess of $50 M_\odot$), and possess the largest radii (15 to $30 R_\odot$; Lamers & Nugis 2002). WNLs are the youngest, coolest and most luminous of the WRs ($>10^6 L_\odot$; Crowther et al. 1995b), and are thought to consist of a helium-burning core and a hydrogen-burning shell (Chu et al. 1983). Early WN stars (WNE) have no hydrogen present in their atmospheres, as it has all been blown off by the wind. Here, as with the WNLs, nitrogen predominates over carbon. However, WNE have smaller radii, and are hotter than the WNL subtypes. WC stars display no hydrogen, and the carbon content of these stars is increased from one part in ten-thousand to 40% by mass as they exit the WN phase (Langer 1990). Stars in a rare and short-lived transition between WN and WC classes are designated WN+WC. WO stars are thought to be descendants of WC stars (van der Hucht et al. 1988), but WOs are very rare; only four of the 298

known Galactic WR stars are WO type (van der Hucht 2006). In general, late types have higher levels of hydrogen in their atmospheres (though all WRs possess very low percentages of H).

Wolf-Rayets, both massive and central star varieties, also have very strong winds (mass loss $>10^{-5} M_{\odot}/\text{yr}$). Wolf-Rayet winds appear to be, for the most part, spherically symmetric. Harries et al. (1998) measured line polarizations in a sample of 29 WR stars with the assumption of a “line effect” in asymmetric stars. This line effect occurs because the polarized continuum emissions of an asymmetric WR star “see” a nonpolarized region as it travels through the surrounding line-emitting matter. Because of this, there is an apparent decrease in polarization at emission-line wavelengths compared to continuum wavelengths in asymmetric stars. Harries et al. found no line depolarization in 80% of the WR stars analysed by linear spectropolarimetry, and therefore sphericity is expected to be a valid assumption at Galactic metallicities (Vink & de Koter 2005). This is one reason for the formation of ring nebulae around Population I WR stars.

1.4.1 General Properties of Massive Wolf-Rayet Stars

All Population I WR stars are hot, with $T_{\star} > 25,000$ K. Central star temperature can, however, take on a large range of values. In the nitrogen class, for example, temperatures are found anywhere upward of 30,000 K for WN10 and approach 100,000 K for early-type WN stars (Abbott & Conti 1987). Stellar temperatures are derived from lines of adjacent ionization states of He or N for WN stars (Hillier 1987, 1988), or from carbon lines for WC stars (Hillier 1989). WR stars are among the brightest in the sky. Absolute visual magnitudes of WR stars are normally obtained from calibrations from cluster membership (van der Hucht 2001). Bolometric corrections range from $M_{bol}-M_V = -2.7$ mag among very late WN stars (Crowther & Smith 1997) to approximately -6 mag for weak-lined, early-type WN and for WO stars (Crowther et al.

1995a,c; Crowther 2000). Luminosities of WN stars range from 200,000 L_{\odot} in early types to 500,000 L_{\odot} in late types (Crowther 2007).

Wolf-Rayet stars are expected to have magnetic fields up to 10^2 G in the case of neutron star progenitors or $\sim 10^3$ G for magnetar formation (Crowther 2007), but fields for other massive WR stars can be considerably lower. One of the first measurements of this quantity was found to be ≤ 25 G for HD 50896, a WR6 subtype star (St.-Louis & Moffat 2007).

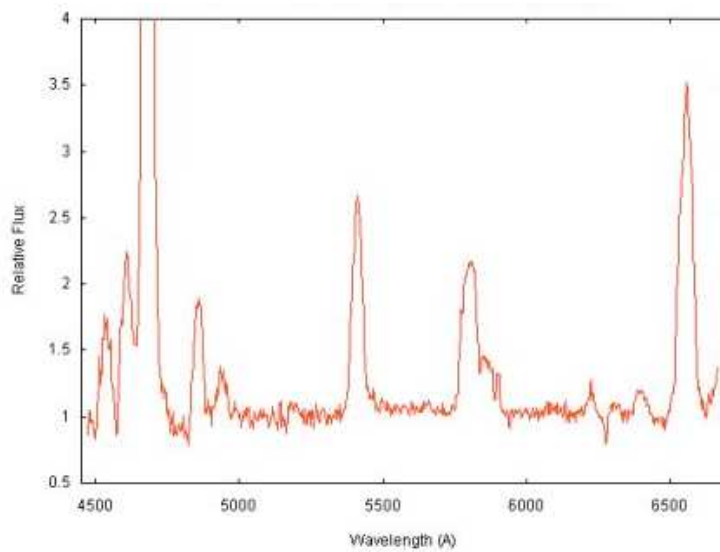


FIGURE 1.5: An example of a Wolf-Rayet spectrum, from star WR1, the first Wolf-Rayet star identified. Note the strong emission lines. Retrieved from <http://www.amateurspectroscopy.com/Astrophysics-spectrum.htm> on 6 March 2008.

1.4.2 Theorized Evolution of Massive Wolf-Rayet Stars

Massive Wolf-Rayet stars follow an evolutionary path very different from their CSPN counterparts, which will be discussed later. It seems as though WRs can evolve from any sufficiently massive star. Wolf-Rayets probably begin their lives as O stars, the most massive stars known. They exhibit high excitation He II $\lambda 4686$ lines, which are indicative of very energetic radiation. They are very hot and luminous, and much of

their spectral energy is radiated in the ultraviolet range.

O stars are the rarest of all main sequence stars; only one in 3 million stars in the solar neighbourhood belong to this class. Some, called the “Of” stars, also exhibit N III lines at $\lambda 4634$ and $\lambda 4640\text{\AA}$, which prove them to be among the hottest of this class (Kaler 1997). These Of stars then evolve into the Ofpe/WN9 class, a designation invented by Walborn (1982) to bridge the gap between true Of stars and true WN9s. The “f” suffix indicates the presence of N III and He II in a star’s spectrum. Likewise, “p” denotes a “peculiar” spectrum, referring to strong spectral lines due to metals. The “e” stands for “emission”, to differentiate from absorption. This class displays high mass loss ($\sim 2\text{--}5 \times 10^{-5} M_{\odot}/\text{yr}$) and slow winds ($\sim 400\text{--}500 \text{ km s}^{-1}$). Their temperatures can range from 30,000–39,000 K, and their radii from 19 to 39 R_{\odot} . From this stage, as the name of the preceding class suggests, a star is expected to proceed into the true Wolf-Rayet class. In most cases (and some researchers say all—e.g. Moffat et al. 1989), the star may, for some time, enter the luminous blue variable stage before returning to the Wolf-Rayet sequence (Langer et al. 1994).

Massive Wolf-Rayets probably represent a stage that is entered when an O-type star sheds its outer layer of H-rich matter (Conti 1976), so that these objects do not pass through an AGB phase. This has become known as the “Conti scenario” since it was first proposed over thirty years ago, and is mostly accepted (see for example Meynet & Maeder (2005), but also Smith et al. (2007)).

Luminous blue variables (LBVs) are very bright stars that exhibit large variations in luminosity and colour and can be related to massive WR stars such as HD 5989 (see Koenigsberger & Moreno 2008). Their lifetimes are relatively short (sometimes only $\sim 40,000$ years) and are characterized by heavy mass loss. They often display P Cygni profiles. P Cygni profiles, which take their name from a star that once exhibited such a spectrum (albeit the eponymous object is no longer a member of this group), are stellar profiles that exhibit strong emission lines accompanied by blueshifted absorption lines.

P Cygni profiles, then, are indicative of rapidly accelerating, rapidly expanding stellar winds, such as are observed around WR stars.

LBV stars may range in temperature from 20,000 K during quiescence to around 8,000 K during periods of maximum brightness. Bolometric magnitudes and luminosities are thought to remain roughly constant throughout these cycles, however; the appearance of cooling is due to absorption of ejected matter into surrounding shells, where the ejecta re-radiate the stellar radiation at longer wavelengths. They vary by 1 or 2 mag over periods of several decades, but on occasion, usually about once every few centuries, LBVs can undergo huge eruptions that increase their brightness by more than 3 mag (Parker et al. 1993). Luminosities of LBVs vary inversely with their periods (Stothers & Chin 1995).

Thus, for massive WR stars, we arrive at a typical evolutionary sequence of O \rightarrow Of \rightarrow H-rich WN \rightarrow LBV \rightarrow H-poor WN \rightarrow H-free WN \rightarrow WC \rightarrow Supernova (Langer et al. 1994). Some (e.g. Norci et al. 1998) place WO stars in between WCs and supernovae. There is also a possible alternative pathway whereby stars around 40 M_{\odot} may become red supergiants or perhaps OH/IR stars, and then proceed to the WR stage (Maeder 1989).

WN and WC stars are, as noted above, the likely progenitors of at least some Type Ib and Type Ic core-collapse supernovae (SNe), respectively (Crowther 2007). This is probable because hydrogen is absent in Type Ib SNe, and hydrogen and helium are absent in Type Ic SNe (Woosley & Bloom 2006).

Direct evidence of this connection is lacking, however, and lower mass interacting binaries are the most probable alternative progenitors. Meynet & Maeder (2005) speculate that observations for confirmation of either of these scenarios within the next couple of years would require around 10^4 WRs, because WR lifetimes are on the order of 10^5 years. According to Hadfield et al. (2005), there are 10^3 WR stars in M83. There are many other galaxies within ~ 10 Mpc besides that could yield the number

necessary to test the supernova hypothesis (Crowther 2007), but ground-based surveys would have very low spatial resolution (20 pc per arcsec at a distance of 5 Mpc).

In any case, light curves of broad-lined Type Ic supernovae taken by Nakamura et al. (2001), Mazzali et al. (2003), and Malesani et al. (2004)—SN 1998bw, SN 2003dh and SN 2003lw respectively—present evidence of ejected core masses of the order of $10 M_{\odot}$. This agrees well with Crowther et al. (2002)’s inferred masses of LMC WC4 stars, if a black hole of several solar masses is supposed to remain (Crowther 2007).

Each of these supernovae were associated with long gamma ray bursts (GRBs), which support the “collapsar” model (MacFadyen & Woosley 1999). In this model, the core of a massive, quickly-rotating Wolf-Rayet star ($> 30 M_{\odot}$) collapses to form a rapidly rotating black hole. In the process, such a star draws in matter at highly relativistic speeds, with a Lorentz factor of around 150 (Crowther 2007). The Lorentz factor is defined as:

$$\gamma = \frac{dt}{d\tau} = \frac{1}{\sqrt{1 - \beta^2}} \quad (1.3)$$

where t represents time in the observer’s rest frame, τ the proper time, and β signifies the quantity $\frac{v}{c}$, where v is the velocity of the object relative to the observer, and c is the speed of light. Thus, if $\gamma = 150$, then this corresponds to matter moving at over 99.997% the speed of light.

The rotational axis of the accretion disk thus formed serves to collimate the gamma ray burst.

Such rotation has been invoked in an attempt at reconciling chemical abundances and mixing rates in observation and theory. The primary driver of such mixing remains unknown, but binarity has been advanced as a possible suspect. While binarity does seem to play an important role in dust formation around massive WC stars, the observed binary fraction among massive Galactic WR stars is only 40% (van der Hucht 2001). Rotation will favour the evolution of a star into the WR phase at earlier stages,

increasing the WR lifetime (Crowther 2007). Spin-down is thought to then follow as angular momentum is lost to the wind. Models that take into account rotational mixing predict better agreements with the observed ratio of WR to O stars at low metallicity, the existence of intermediate WN/C stars, and the ratio of blue to red supergiants in galaxies (Crowther 2007). Rotation could also remove the need for a binary system scenario for the formation of Wolf-Rayets. While models with binarity and no rotational mixing, carried out by Eldridge & Vink (2006), find better matches to stars of higher metallicities, Meynet & Maeder (2005) find that including rotation removes this requirement.

Rotation is difficult to measure in WR stars because photospheric features usually employed to calculate $v \sin i$ are not observable beneath the optically thick wind. (Here, v represents the tangential velocity of a star, and i represents the angle between the axis of rotation and the line of sight connecting the star to the Earth. Therefore, the quantity $v \sin i$ serves as a lower limit of the true velocity of the body.) Velocities of between 200 and 500 km s⁻¹ were inferred for WR138 by Massey (1980) and for WR3 by Massey & Conti (1981). However, these probably do not reflect actual rotational velocities, since the first has a binary companion while the second was observed only by means of stellar wind lines (Marchenko et al. 2004). While some WR stars do possess large-scale line-profile variability (LSLPV) which may be used to determine rotation period (St.-Louis & Moffat 2007), this is by no means common.

If WR stars had fast rotations in general, a line polarization effect could be observed, brought about by gravity darkening, a process whereby gas at the equator of a star, due to its centrifugal motion, is rarefied and thus decreases in pressure, temperature, and brightness (von Zeipel 1924; Owocki et al. 1996). However, upon examining linear spectropolarimetric data for twenty-nine Galactic WR stars, Harries et al. (1998) found that only four WN stars and one WC+O binary showed a line effect indicative of significant asphericity. Their radiative transfer models suggested that the observed

polarizations could be matched with an equator-to-pole density ratio of between 2 and 3. As suggested by the limited number of WR stars showing the line effect in the sample of Harries et al., most Milky Way WR stars do not show a strong linear polarization line effect (e.g. Kurosawa et al. 1999). WR CSPNe would also be expected to exhibit a low ratio of rotating stars, considering that their heavy mass loss should serve as an efficient method for disposing of angular momentum.

There is a strong correlation between WC subclass and line width, earlier subtypes having larger line widths (Torres et al. 1986), as well as a correlation between higher metallicity and broader lines, suggesting faster winds. Earlier WC types tend to be observed at lower metallicity, which led Smith & Maeder (1991) to suggest that early WC stars are more carbon-rich than late WCs. Koesterke & Hamann (1995) examined a sample of 25 Galactic WC5-8 stars, but were unable to confirm any subtype-carbon abundance relationship. Crowther et al. (2002) supported the conclusions of Koesterke & Hamann, finding that the range of (C+O)/He abundance ratios in LMC WC4 stars were similar to those of Galactic WC5-8 stars, but these are different galaxies, and therefore a new study of this relationship is warranted. WC9 stars do not necessarily exhibit weaker winds than earlier subtypes, but they truly possess lower temperatures (T_{eff} at $\tau_{Rosseland}=20$; Crowther et al. 2006).

Smith et al. (1994) extended the WN subtype sequence to include very late types, designated as WN10 and WN11. This change in the classification enabled them to include a group of emission line stars that had been previously classified as Ofpe/WN9 by Bohannan & Walborn (1989). WN11 subtypes greatly resemble very early-type B supergiants, but lack emission at He II $\lambda 4686$.

For those rare cases where the C IV doublet at $\lambda\lambda 5801,12$ appears unusually strong in a WN star, Conti & Massey (1989) have created an intermediate WN/WC classification.

The above description of the generic massive star WR class and their fundamental

properties must be appreciated when their CSPN cousins are studied, as the physical conditions present in both types are similar, and understanding of one can provide insight into the other. There are some important differences of course, and these are touched on below.

1.5 Wolf-Rayet Central Stars of PNe and their classification

Among the central stars of PNe is a group which exhibits the tell-tale spectral hallmarks of massive Wolf-Rayet (WR) stars. These central stars are generally denoted as [WR] or WR CSPNe (for Wolf-Rayet Central Stars of Planetary Nebulae) and comprise roughly 10% of all CSPNe: 15% in the galactic bulge and $\sim 6\%$ in the disk, suggesting that higher metallicities are conducive to new [WR] PN formation (Górny et al. 2004).

Such [WR] CSPNe are relatively rare; only around 103 are known in the Milky Way, of which 30 have been discovered by MASH, including those arising from the work described in this thesis. Note that exact numbers are difficult to quote, as some objects may be classified as weak emission-line stars (WELS) by other observers. There are also two [WR]s known in the Small Magellanic Cloud (SMC) and five in the Large Magellanic Cloud (LMC; Parker et al. 2006; Peña et al. 1997c). In addition, three are known to belong to the Sagittarius Dwarf Galaxy (Walsh et al. 1997; Zijlstra et al. 2006).

[WR] stars are, like their massive counterparts, divided into basic [WC] and [WO] types. There is a third proposed classification of [WN] stars which, although common in massive WR stars, are exceedingly rare among [WR]s. Their existence is far from universally accepted. Furthermore, unlike massive Wolf-Rayets, most [WR]s are [WC], and relatively few are of [WO] type

These types are further subdivided into groups designated by Arabic numerals after

the [WN], [WO] or [WC] designation, following the same convention as their Population I counterparts. All are defined by relative line strength ratios, with smaller numbers indicating earlier types and larger numbers later types. It is evident that subtypes [WO1] and [WC10-11] are unique to [WR] CSPNe (Crowther et al. 1998) with no counterparts found among the massive equivalents. It is also noteworthy that Górný et al. (2009) suggest that [WC11] stars are evolutionarily distinct from both Weak Emission Line stars (WELS) and [WR] stars. They arrive at this conclusion by modeling the masses of the various nebulae and their central stars. They find that [WC11] central stars and nebulae are less massive than other [WR] types. In addition, Gesicki et al. (2006) find that the only [WR]s in their sample to not show indications of turbulence are [WC11] stars. Recall that all progenitor central stars of PNe possess relatively low initial masses from $\sim 0.8 - 1.0$ to $\lesssim 8 M_{\odot}$. The wind of a larger, more massive and luminous star would blow away this matter too quickly. Wolf-Rayet central stars of PNe are distinguished by strong, broad emission lines indicative of high-excitation nitrogen, carbon or oxygen lines, depending on the type of the star—[WC] or [WO]—in addition to the narrower nebular emission lines. [WC] types also emit strongly at C III $\lambda 4650$. See Figure 1.6 for examples of [WC] spectra.

The reason why some CSPNe develop into [WR] stars and others do not is unclear. However, it is apparent that there must be some mechanism to remove all or most of the surface hydrogen through burning or mass loss (refer to above section on evolution of the massive equivalents). The most widespread view of [WR] CSPN evolution is that late types evolve into early types, which then eventually progress into a PG 1159 stage, wherein they cool and exhibit He, C and O absorption lines on their way to becoming white dwarfs (see e.g. Werner & Herwig 2006). Evolution between subclasses is comparatively rapid for these stars. Based on contrasts between X-ray and optical/near-infrared imaging, it is assumed that [WCL]s and their PNe evolve between subclasses on timescales of less than 5000 years (Akashi et al. 2006).

1.6 Taxonomy of Hydrogen-Deficient Central Stars of PNe

As mentioned above, [WR]s, WELS and PG 1159 stars are generally partitioned according to the carbon and nitrogen features in their spectra. Late-type [WR]s will exhibit the C III $\lambda 5696$ line and, depending on the subclass, C IV $\lambda\lambda 5801,12$ to varying degrees, with earlier subclasses possessing higher C IV to C III ratios. The hottest [WR]s—the early subtypes—will exhibit weak to no C III $\lambda 5696$. WELS exhibit highly ionized winds, presenting a C IV $\lambda\lambda 5801,12$ doublet with equivalent widths of less than 10 \AA (Tylenda et al. 1993). Furthermore, these objects exhibit an emission feature around 4650 \AA , owing to the presence of N III $\lambda\lambda 4634,4641$, C III $\lambda 4650$ and C IV $\lambda 4658$. C III $\lambda 5696$ is usually very weak or absent, owing to the high ionization of the wind. He II $\lambda 4686$ is sometimes visible. PG 1159 stars will, by contrast, exhibit an absorption feature around 4670 \AA due to the He II $\lambda 4686$ and C IV $\lambda 4658$ lines, as mentioned above.

Several close binary central stars show spectra similar to those of the WELS (De Marco et al. 2008), presenting with emission lines in the area of the 4645 \AA complex and C IV $\lambda 5801,5812$. However, some close binaries possess C III $\lambda 5696$ and C IV $\lambda\lambda 5801,12$ lines of similar intensities, which could serve to distinguish these objects from actual WELS. Some examples of close binary planetary nebula nuclei (PNNi) with such spectra are Abell 46 (Pollacco & Bell 1994), LTNF 1 (Ferguson et al. 1987), DS 1 (Hilditch et al. 1996) and the Necklace Nebula (Corradi et al. 2011). Relevant line ratios are included in the respective papers.

Some CSPNe have been classified as both Of and WELS in the literature. Of CSPNe are spectroscopically analogous to those massive stars which are designated Of by Walborn (1971). These stars possess N III $\lambda\lambda 4634,41$ as well as He II $\lambda 4686$ in emission. Those stars that possess only these N III emission lines, but lack the

He II $\lambda 4686$ line, are denoted O(f), and those stars that exhibit N III $\lambda\lambda 4634,41$ in emission but have an absorption line at He II $\lambda 4686$ are termed O((f)). Other H-rich CSPNe have only C IV lines in emission, e.g. NGC 1535 and NGC 4361 (Mendez et al. 1981). A proper classification is therefore dependent on sufficient spectral resolution and sensitivity, as well as the spectral coverage (Mendez et al. 1988, 1990).

In light of this, the WELS are probably an inhomogeneous class, comprised of at least three different groups: (i) H-rich stars with weak emission lines which would be classified as Of or O(f) at sufficient spectral resolution, (ii) H-deficient stars with winds that are considerably weaker than those of [WR]s, and (iii) misclassified binary central stars, whose emission lines arise from the irradiated hemisphere of a cooler companion. Groups (i) and (iii) would appear H-rich.

The examination of different populations of H-deficient CSPNe may seem straightforward at first, but there are several complicating factors involved in the identification of class and subclass. Blue spectra are very important for proper identification in order to look for the presence of the N III $\lambda\lambda 4634,4641$ lines in WELS and the 4670\AA feature in PG 1159 stars. In some cases, it is possible that the presence of a red spectrum exhibiting a C IV $\lambda\lambda 5801,12$ doublet feature, along with other high-ionization carbon and oxygen lines, may lead an observer to assume that the observed object is actually an early-type [WC] or a [WO] star when it should actually be classed as a WELS, as the observer assumes the absence of the N III $\lambda 4634$ and $\lambda 4641$ lines. This is especially the case when extinction prevents the detection of the blue lines. Lack of even bluer spectra can hamper the proper identification of [WO]s through the broad 3818\AA feature. It is important in any case to measure the EW of the C IV $\lambda\lambda 5801,12$ doublet lines, taking into account that lines with equivalent widths of less than $\sim 10\text{\AA}$ suggest a WELS classification.

1.6.1 Theorized Evolution of Wolf-Rayet Central Stars of PNE and Thermal Pulse Scenarios

As mentioned earlier, [WR] PNe possess much smaller core masses and radii than their massive counterparts. While the massive types seem to evolve from much larger stars of greater than 25 solar masses, WR CSPNe appear to descend from AGB stars of $\sim 1-8 M_{\odot}$ (Crowther et al. 2006). [WR] central stars, because of their smaller surface area, appear with lower luminosities than their massive counterparts, in accordance with their post-AGB origin (Montez et al. 2005).

The process sparking the AGB/post-AGB \rightarrow [WR] transition in single stars has been much debated (see Koesterke 2001, for summary). There are three of these possible scenarios (as described in Herwig 2001): the Late Thermal Pulse (LTP), Very Late Thermal Pulse (VLTP), and Asymptotic Giant Branch Final Thermal Pulse (AFTP).

LTP occurs when the star has left the AGB and is still burning hydrogen in a shell. Hydrogen at the surface is at first unchanged by the pulse, but later dredge-up mixes the H downward, resulting in a compositional component of several percent hydrogen which remains on the surface. It should be noted here that in this case, the hydrogen deficiency is a result of dredge-up mixing, and not actual burning of the hydrogen.

VLTP occurs late in the post-AGB phase when H-burning has already ceased. In this case, convection mixes hydrogen downward (a process referred to as the hydrogen ingestion flash or HIF), where it is burned, resulting in an H-free surface. AFTP happens during a thermal pulse at the end of the AGB and involves only a small H-shell mass. H-burning ceases and hydrogen is mixed downward, but this time it is not burned and the remaining hydrogen abundance is relatively high.

If N is detected in the spectrum of a star, a VLTP origin is considered likely, because this is a product of H-burning, whereas C predominance signifies He-burning and a more evolved state (Crowther 2007). An overabundance of Ne is associated with a VLTP, owing to the extensive burning of other elements in this scenario (Todt et al. 2008).

Likewise, if little He can be detected, this is indicative of an LTP origin (Parthasarathy et al. 1998). LTP stars have no Li production, no enhanced ^{14}N abundance, and a larger $^{12}\text{C}/^{13}\text{C}$ ratio than in VLTP hydrogen-ingestion flash (HIF) models. After LTP, the star will have a nitrogen content no greater than 0.1%, but VLTP stars will have several percent (Werner & Herwig 2006). Thus, all of these situations provide a means of determining a hypothetical life history of the star.

Different stars exhibit different hydrogen abundances, thus suggesting that there may not be only one evolutionary sequence for [WR] stars. It must be noted, however, that Górný & Tylenda (2000) conclude that VLTP is not a major evolutionary path to the [WC] stars based on their models. They state that while H-deficient PN nuclei mostly evolve from the AGB, they were unable to make the mass-loss as efficient as it needed to be to create this situation in their models.

Leuenhagen et al. (1996) and Leuenhagen & Hamann (1998) find abundances of neon and nitrogen in [WCL] stars consistent with the VLTP scenario. They also found typical $X_C : X_{He}$ (C:He number ratio) of 50:40, also supportive of the VLTP. However, Todt et al. (2008) point out that the 10% hydrogen composition is indicative of an AFTP or LTP origin. (This hydrogen abundance determination is not unquestioned. De Marco et al. (1997) examines line profiles and suggests that the Balmer lines may be emitted by the nebula and not the stellar wind.) Upon analysing a sample of [WCE] stars, Todt et al. (2008) could not fit the Ne lines, but found an overabundance of N of 1 to 2% in their models. The only scenario in which Werner & Herwig (2006) find an overabundance of N is the VLTP. They found lower C abundances in [WC2] stars compared to [WCL] types, as well as a decreased $X_C : X_{He}$ ratio of 30:50, which further suggest that [WCL] stars do not evolve into [WCE]s. Furthermore, these C abundances support the AFTP scenario. To make matters more difficult, we also have weak-emission line stars (WELS), which exhibit emission lines at many of the same wavelengths as WR and [WR] stars, but these features are neither very broad nor very

prominent. Their origin is still being debated. (See section on PG 1159 and WELS stars below.) Thus, at the moment the evolutionary picture is still rather confused and improved clarity here is one of the primary aims of this thesis.

As noted above, [WN] stars are very rare, with only two having been discovered to date: N66 (Peña et al. 1995) and PM5 (Morgan et al. 2003). The central star of PB8 has also recently been classified as a [WN/WC] type (Todt et al. 2010). However, the surrounding nebulae and environment of these stars are very different. N66 resides in the LMC and is bipolar, whereas PM5 is a Galactic [WN] and appears to be spherical. PB8 is a Galactic bipolar nebula. PM5 is an object found in the SHS. However, the observational data for this object is somewhat contradictory and this object may actually turn out to not be a PN. Refer to Chapter 4 for more details on the putative [WN] and proposed [WN/WC] subclasses.

Peña et al. (2003a) found that nebulae surrounding [WR] stars are in general much more nitrogen-rich than PNe with WELS and other non-WR central stars. Furthermore, none of their WELS nebulae showed any evidence of N-enrichment. This is in line with the finding of Fogel et al. (2003) that WELS are simply less massive, less luminous, and weaker-lined cousins of [WR] PNe. Their smaller masses would seem to inhibit the hot-bottom burning (HBB) which is necessary for nitrogen enrichment. Boothroyd et al. (1995) found that their models of AGB stars between $\sim 4.5\text{--}7M_{\odot}$ initiated HBB, producing envelopes with ratios of $\frac{^{18}\text{O}}{^{16}\text{O}} \leq 10^{-6}$ and $\frac{^{17}\text{O}}{^{16}\text{O}} \leq 10^{-1}$. There is, however, another potential pathway to nitrogen-enrichment which may affect stars below $2.5M_{\odot}$. Extra thermohaline mixing may occur in these low-mass stars in the red giant phase, causing extra CNO products to appear at the surface (see e.g. Charbonnel & Zahn 2007; Eggleton et al. 2008; Stancliffe 2010). This would significantly increase the proportion of stars that display nitrogen features, as the high-mass HBB stars are in the minority.

1.6.2 The Born Again Scenario

The evolutionary pathways to the observed [WR] subclasses are far from clear, though various possible mechanisms have been put forward as briefly described below.

One theory for [WR] CSPNe formation, the so-called “Born Again” scenario, was advanced by Iben et al. (1983) to explain two objects, A30 and A78. In this scenario, a star has already assumed a white dwarf configuration and begun tracing a path down the white dwarf cooling sequence. It is at this point that convection drives the He ash upward and the white dwarf undergoes a final thermal pulse, which mixes the hydrogen from the outer layers down into the helium-burning shell. The hydrogen is then completely burned. Following the pulse, the star expands to the size of a red giant for a brief period and continues to burn helium in a shell, approximately retracing the same path it followed as the star continued to burn hydrogen during the initial excitation of the surrounding nebula. Thus, this scenario traces out a second loop on the H-R diagram.

Candidates for this scenario have lower nebular electron densities ($\sim 3600 \text{ cm}^{-3}$) than other nebulae of similar [WC] type (Peña et al. 2001). Only five objects are believed, at present, to be examples of this process: Abell 30 and Abell 78 as originally suggested by Iben et al. (1983), Sakurai’s Object (V4334 SGR; e.g. Miller Bertolami & Althaus 2007), and V605 Aql and FG Sge (Clayton & De Marco 1997). Sakurai’s Object agrees with the born-again theory of a VLTP star, but mixing efficiency must be reduced from current assumptions by a factor of ~ 100 in order for the models to replicate the phenomenon on the observed time scale (Miller Bertolami et al. 2006). Mixing in stellar interiors is not well understood at this point, so it is not clear whether this new mixing efficiency is realistic. Chesneau et al. (2009) find that Sakurai’s Object is most likely a binary object.

1.6.3 PG 1159 and WELS Stars

There are two types of stars that are important for the study of [WR] stars, even though these objects do not fall into the same category. The first of these are PG 1159 stars. PG 1159 stars appear to comprise an intermediate stage between [WCE] and white dwarfs. PG 1159s are CSPNe characterized by hydrogen-deficient atmospheres and high temperatures (75 kK to 200 kK), as well as absorption lines for He, C, and O (Werner & Herwig 2006). There is also another class defined by Koesterke (2001) which includes those stars that show clear signatures of stellar winds in the UV but resemble PG 1159 stars in the optical ([WC]-PG 1159 stars). Note that not all PG 1159 stars have a detectable external nebula.

The second stellar type is the weak emission-line star (WELS). These stars, as their names suggest, exhibit narrower and weaker emission lines at WR-characteristic wavelengths (Marcolino & de Araújo 2003). As is mentioned in other parts of this review, WELS are not considered to be part of the evolutionary sequence of [WR] stars. They appear instead to be lower mass stars that evolve in the same way as their more massive [WR] and WR cousins, unable to generate the same wind strength, but are otherwise very similar. Górný et al. (2009) find that while WELS are usually found within Galactic longitudes of 4.5° , [WR] PNe are generally located further away. WELS, like the [WR] PNe, also exhibit values for $T_e(\text{O III})$ that are on average lower than 0.1 dex below those for normal PNe (Górný et al. 2009).

PG 1159 stars show evidence of surface compositions similar to [WR] stars, but they exhibit less mass loss (Koesterke & Hamann 1997b). They also show no signs of hydrogen, leading some to assume an LTP origin (Parthasarathy et al. 1998). This proposed evolution is supported by higher abundances of hydrogen in late types (between 1 and 10%) as compared to early types, where often none is found (Werner & Herwig 2006; Leuenhagen & Hamann 1994). Determination of hydrogen content is difficult, however, owing to the facts that: 1) the broad H lines are always blended

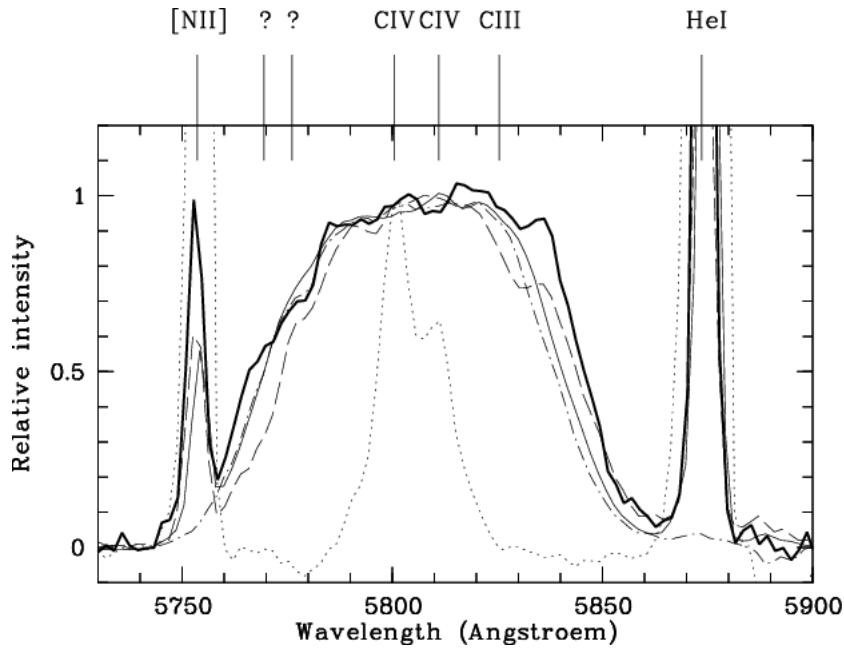


FIGURE 1.7: This figure, from Acker & Neiner (2003), shows the drastic difference in linewidth between several [WO4]pec stars and a WELS star. The thick line gives the spectrum for M 1-51, the thin solid line Cn 1-5, M 1-32 the dashed line, and PM 1-89 the dashed-dotted line. The dotted line shows the spectrum of M 1-61, a WELS star, for contrast.

with He II lines due to high terminal velocity and 2) completely removing H I emission lines by data reduction is impossible (Koesterke 2001). Carbon abundance in [WCL] stars is 0.50 by mass, but only reaches 0.25 in [WCE]s (Koesterke 2001). Werner & Herwig (2006) suggest that systematic errors may play a role here, seeing as different spectral lines are used to obtain abundances in these two classes. Nonetheless, they believe that similar He/C ratios in PG 1159 and [WC] stars justify this sequence. See also De Marco & Barlow (2001) for further analysis of modeled abundances and their arguments for the different origins of [WCE] and [WCL] stars. Crowther et al. (2003) find that better observations and the inclusion of clumping and line blanketing in the models can however reconcile the carbon discrepancy; they find that [WCL] carbon abundances are not systematically higher than those of [WCE]s.

Some place WELS between the early [WR] types and PG 1159 stars (e.g. Parthasarathy

et al. 1998; Marcolino & de Araújo 2003). These objects are in general less ionized than WR CSPNe, but nonetheless still exhibit one or more of the characteristic [WR] emission lines at a much reduced level. The most important features of these stars are the 4650 Å blend and the C IV $\lambda\lambda 5801, 5812$ doublet (Marcolino & de Araújo 2003). The placement of the WELS in the evolutionary pathway championed by Parthasarathy is, however, disputed by several papers. Peña et al. (2001) and Girard et al. (2007) in particular cite lower N/O and He/H ratios in WELS as evidence that they form from smaller progenitor stars and do not belong to the same sequence as [WR] CSPNe. Others believe that WELS exhibit hydrogen (Peña et al. 2001), which they take as evidence that WELS do not belong to this sequence. WELS do, on the other hand, exhibit certain interesting similarities to WR CSPNe. Peña et al. (2001) argue that while WELS PNe are more similar to ordinary PNe than to [WR] PNe, in an examination of six WELS, they found that these objects still follow the same wind density versus [WC]-type relation as true [WR] PNe, but that WELS also tend to have smaller expansion velocities.

The data of Peña et al. (2003b) supported the hypothesis that [WR] PNe do indeed expand faster than non-[WR] PNe. They also found that WELS winds expand at the same rate as those of non-[WR] PNe, again suggesting that WELS are not in any way involved with the [WR] evolutionary sequence. A weak correlation between stellar temperature and wind velocity was found in the [WR] PNe sample. Peña et al. believed this to possibly be a result of older stars having higher temperatures. Although a similar correlation was found in the non-[WR] PN objects, it was less pronounced than that of the [WR] PNe. Gesicki & Zijlstra (2000) found no such relationship, indicating that if this correlation is in fact real, it is probably very small.

[WR] Subtype Distribution

Galaxies also appear to differ in their [WR] subtype distribution, which could indicate some influence of inherent system metallicity. In the Magellanic Clouds, all of the [WR] stars fall within the [WC4-5] and [WC8] spectral types, whereas Galactic objects tend to be concentrated in the [WO3-4] and [WC8-11] subtypes, with very few in the intervening classes (Peña et al. 1997c; Tylenda et al. 1993). Furthermore, the [WR] PNe in the MCs are of relatively low excitation and have large electron densities ($n_e \geq 10^4 \text{ cm}^{-3}$; Peña et al. 1997c), indicating that these objects are fairly young. These subtype distinctions also imply different kinds of radiation, specifically in the dichotomy of hard or soft ionization. Hard ionization involves incident photons so energetic that, upon impact with matter in the wind, they break molecules apart, or eject electrons from their atomic orbits, thus giving rise to many highly excited species. Soft ionization is readily absorbed by matter in the wind, converting that energy more fully into outward motion instead of bond-breaking and particle ejections.

Cooler [WC] CSPNe have a tendency to not reside in bipolar or spherical nebulae, but rather elliptical PNe (De Marco & Soker 2002). The least ionized, most luminous members of this group, the [WCL] (see below for discussion of subtypes) stars, possess smaller, denser nebulae of radii $< 0.015 \text{ pc}$, indicating a short evolution time (Girard et al. 2007). Interestingly, the only Galactic [WN] star known, PM5, belongs to a well-defined spherical nebula, though this may not even be a PN (Morgan et al. 2003). Morphology is rendered even more difficult to explain in light of the finding of Peña et al. (1998) that PNe with nuclei of the same [WC] subtype may have very different nebular properties (e.g. morphologies and abundance ratios), indicating that stars with very different initial masses can pass through the same [WC] stage. The exact processes by which these varying morphologies manifest themselves are still unknown, though there are several clues. Stanghellini et al. (2003) found, in comparing the populations of LMC and SMC PNe, that low metallicity somehow discourages the formation of

bipolar nebulae. Interestingly, the MASH survey of Parker et al. (2006) reported a much higher fraction of circular and near circular PNe ($\sim 45\%$) compared to previous estimates, such as 10% from Soker (1997).

1.6.4 Modeling of [WR] Stars

PNe with [WR] central stars have been modeled in many different papers. Clumping phenomena are discussed extensively in the literature, because WR winds are highly clumped owing to the large amounts of matter that they throw off (Moffat & Robert 1994). One very important parameter in these calculations is the transformed radius (R_t). This quantity was first defined by Schmutz et al. (1989) as:

$$R_t = R_\star \left[\frac{v_\infty/2500 \text{ km s}^{-1}}{\dot{M}} \sqrt{f}/10^{-4} M_\odot/\text{yr} \right]^{2/3} \quad (1.4)$$

where f is the clumping factor. Stars with the same stellar temperature, transformed radius, and chemical abundances exhibit very similar spectra irrespective of actual stellar radius, mass loss and terminal velocity (Schmutz et al. 1989). The smaller the transformed radius, the greater the wind density. Here $\rho_{avg} = f \rho_{clump}$. Ionization structure of a clumped wind will behave similarly to that of an unclumped wind with a \sqrt{f} times lower mass-loss rate. Also, observed emission line spectra are almost invariant for the ratio \dot{M}/\sqrt{f} (Vink & de Koter 2005). Marcolino et al. (2007b) therefore believed clumping could account for the observed difference between WELS and [WR]s in their models, though others are skeptical of this. As mentioned earlier, WELS appear to simply be less massive versions of [WR] stars, and thus clumping would probably be insufficient to bridge the gap between these two groups.

Modeling is also important to calculate mass-loss rates. Causes for an increase of the mass-loss rate include an increased C/He ratio, a decrease in terminal flow velocity, and more rapid wind acceleration (Vink & de Koter 2005).

1.7 Conclusion

PNe in general are very important in the evolution of the Galaxy, as they recycle old matter and disperse newly created elements, which ultimately enrich the gas out of which new star systems form. It is crucial to our understanding of stellar life cycles to know what different pathways a star's chemical evolution may take, and what causes different abundances in stars. The Wolf-Rayet central stars, along with other H-deficient descendants of main sequence stars, should be examined in particular to aid us in this objective.

2

Data Reduction

*We mounted up, he first and I the second,
Till I beheld through a round aperture
Some of the beauteous things that Heaven doth bear;
Thence we came forth to rebehold the stars.*

—Dante Alighieri, *Inferno: Canto XXXIV*

Overview

In any scientific examination, evidence is required to make a case. Therefore, the proper preparation of the analyzed data is of the utmost importance. With this in mind, I present a description of the data reduction procedures undertaken during the course of this thesis. All data presented in this thesis, when not obtained from other on-line catalogues or literature sources, were taken on the 2.3 Metre Telescope at Siding Spring Observatory, first using the Dual Beam Spectrograph (DBS) and then the Wide Field Spectrograph (WiFeS; Dopita et al. 2010), after its commissioning in the autumn of 2009. Further spectroscopic data was obtained for this programme during service observations on the Anglo-Australian Telescope (AAT) of the Australian Astronomical Observatory (AAO) using both the 2dF/AAOmega multi-fibre system and the SPIRAL integral field unit (IFU). This chapter will outline the standard spectroscopic reduction steps taken while dealing with data from each of these telescopes and associated spectrographs. Note that for the AAO the latter two instruments have highly sophisticated automated or semi-automated spectroscopic reduction pipelines available that were employed wherever possible. They accomplish the same general tasks as many other spectroscopic reduction packages. Extensive use was also made of the IRAF software, especially for the DBS data following the general techniques (see below).

2.1 The Dual Beam Spectrograph

The Dual Beam Spectrograph (DBS; Rodgers et al. 1988) was built in the 1980s and operated for over twenty years, mounted on the Nasmyth A focus of the 2.3 Metre telescope at Siding Spring Observatory. As its name suggests, it consisted of two 150 mm collimator beams. See Fig. 2.1.



FIGURE 2.1: A picture of the DBS, mounted on the 2.3 Metre telescope. The blue arm is to the left and the red is to the right.

2.2 Basic Spectroscopic Data Required

For any spectroscopic observing mission, certain minimal types of exposure are usually required, regardless of whether the data is long-slit (as in the case of the DBS data), multi-object (as for 2dF/AAOmega) or where areal spectroscopic data is acquired for extended objects as with an integral field unit or IFU (SPIRAL) or image slicer (WiFeS). These basic exposures are bias frames, dark frames (less important these days), flat-field frames, sky flats, calibration frames and target object frames. The exact form, importance and number of these exposure types varies among the various instruments according to such factors as CCD and spectrograph performance and stability, etc. The importance and function of each of these basic exposure types when undertaking astronomical spectroscopy are briefly summarised below. See Fig. 2.2 for examples.

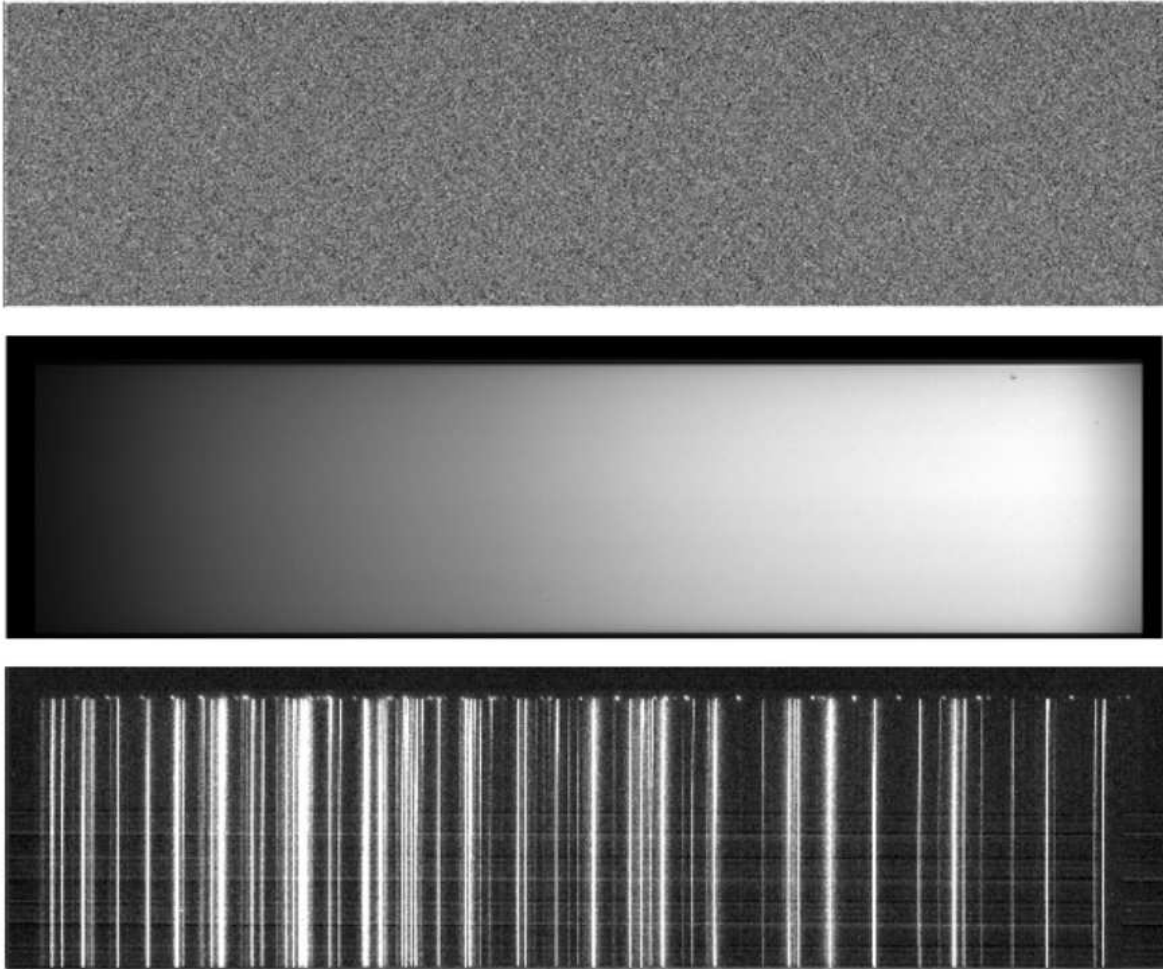


FIGURE 2.2: Example frames taken on the 2.3m in May 2008. At top is a bias frame. The noisy nature is apparent. The middle frame is a flat-field taken with a quartz lamp. The illumination is smooth, as the lamp emits a continuum of wavelengths. This is in contrast to the example arc lamp exposure at bottom, which clearly shows the distinct wavelengths produced in the gas.

2.2.1 Bias Frames

Often significant numbers of bias frames are taken before being averaged and used to subtract off the bias level from the other exposure types. The bias image represents the thermal noise on the CCD, caused by the random movement of the molecules that make up the detector. Liquid nitrogen is often used to cool the chip and thus minimize

this noise, but it is impossible to completely eliminate it. For this reason, a number of bias frames are taken and averaged together. This will eventually be subtracted off of the target frames.

2.2.2 Dark Frames

During long exposure times CCD detectors can accumulate charge (fixed-pattern noise) that adds an additional low-level signal over and above the normal bias level that needs to be subtracted. With the most modern detectors, the dark counts have become very low such that these exposure types are often ignored or taken rarely during an observing run.

2.2.3 Flat-Field Frames

Flat-field frames are usually taken using a full-spectrum, incandescent light source such as a quartz lamp, which is shown onto a screen either within the telescope cover itself, or on a screen located on the inner surface of the telescope dome. These exposures are used to determine the response across the entire CCD, so that portions that receive only relatively little light can be calibrated such that the entire image or spectrum will have the correct relative intensities.

2.2.4 Sky Flats

Sky or twilight flats are taken at sunset or sunrise, just as the sun sits below the horizon. These exposures provide us with a spectrum of telluric lines which originate in Earth's atmosphere, as opposed to the target. These will also be subtracted off of the target frames.

2.2.5 Calibration Frames

All spectroscopic data needs to be calibrated. This is usually accomplished by arc lamp exposures taken to accompany the target frames. Arc lamps provide a rich emission line spectrum of known species (e.g. copper-argon, iron-helium) which have precise emission wavelengths previously determined in the lab. Specific wavelengths will register on a set point along the dispersion axis of a detector, and by observing the ensemble of lines produced by the arc lamp, we can fit a function to the CCD so that we know what wavelength a line possesses.

2.2.6 Target frames

The target frames are of course essential. From these frames we subtract contributions of the bias and dark frames and sky lines, then wavelength- and flux-calibrate the spectrum.

2.2.7 Cosmic Rays

Cosmic rays are subatomic particles from space that, due to their high energy, are able to pierce the Earth's magnetosphere and enter the atmosphere. "Primary" (original source) particles and "secondary" particles resulting from collisions of the primary with others in the atmosphere will impact the CCD frequently enough that it is necessary to clean the plate; otherwise these events will contaminate the spectrum, resulting in a spurious emission line when the spectra are binned and reduced to two dimensions.

2.2.8 Spectrophotometric Standard Stars

Observations of spectrophotometric standard stars were routinely made as part of general observing strategy and especially in good photometric conditions. Observations on the DBS in particular included such observations regularly throughout the night.

Spectrophotometric standards have well-known flux distributions as a function of wavelength; these are used to apply a flux calibration to the target data. This enables us to determine meaningful Balmer decrements and emission line ratios from the spectra. These stars were selected from the list of Dopita & Hua (1997).

2.3 Spectroscopic Data Acquired During This Thesis

In the course of this thesis, various observing missions were undertaken to hunt for more examples of [WR] CSPN from the general MASH survey and/or to follow-up specific discoveries to obtain better data in terms of both improved S/N, resolution or wavelength coverage. Table 2.1 summarises all these spectroscopic observing missions that have contributed to the results presented in this thesis. Column 1 gives the Telescope used, column 2 the instrument, column 3 the dates of observation and column 4 the observers.

2.4 The Image Reduction and Analysis Facility; IRAF

The majority of our data was processed using the Image Reduction and Analysis Facility (IRAF), which is written and supported by the National Optical Astronomy Observatories (NOAO) in Tucson, Arizona, United States. NOAO is operated by the Association of Universities for Research in Astronomy (AURA), Inc. under a cooperative agreement with the National Science Foundation (NSF). IRAF software is well-known and widely used by astronomers. New IRAF versions and information on installation, use and troubleshooting can be found at <http://iraf.noao.edu/>. The standard spectroscopic reduction steps as outlined in the manual “Reducing slit spectra with IRAF” (<http://iraf.noao.edu/docs/spectra.html>) were closely followed. Also, and specifically

TABLE 2.1: A summary of observing runs carried out in the course of this thesis. Spectral resolution and wavelength coverage varied according to the specific gratings used on the night. Please refer to later chapters for details on these values.

Telescope ¹	Instrument	Dates	Observer ²
2.3m	DBS	12-18 Nov 2007	AK, KD
2.3m	DBS	6-15 May 2008	KD, BM
2.3m	DBS	6-11 Jun 2008	KD, KV
2.3m	DBS	4-7 Jul 2008	KD
2.3m	DBS	1-5 Aug 2008	KD
1.9m	CCD SPEC	17-24 Dec 2008	QP, KD
2.3m	DBS	14-18 Jan 2009	KD
AAT	SPIRAL	13 Jun 2009	RS
2.3m	WiFeS	27 Jun–1 Jul 2009	DF, RB
2.3m	WiFeS	19-23 Apr 2010	KD

¹2.3m=2.3 Metre (Siding Spring Observatory), 1.9m=1.9 Metre (South African Astronomical Observatory), AAT=Anglo-Australian Telescope (Siding Spring Observatory). ²AK=Anna Kovacevic, BM=Brent Miszalski, DF=David Frew, KD=Kyle DePew, KV=Kerttu Viironen, QP=Quentin Parker, RB=Richard Baxter, RS=Rob Sharp.

for PN work, the IRAF add-on package and associated DS9 visualisation infrastructure developed for the MASH project by Brent Miszalski called the Planetary Nebula Data Reduction (PNDR) pipeline was also employed (<http://star.herts.ac.uk/brent/pndr/>).

2.4.1 Reduction of DBS Data

The majority of data taken in the course of this thesis was taken on the 2.3 Metre Telescope at Siding Spring Observatory approximately 40 kilometres west of Coonabarabran, New South Wales, Australia in the Warrumbungle National Park. The observatory rests on Siding Spring Mountain, at a height of approximately 1165 m (3822 ft) above sea level. This is also the site of the AAT, which will be briefly detailed later on in this chapter. The following data reduction process is illustrated in Figure 2.3.

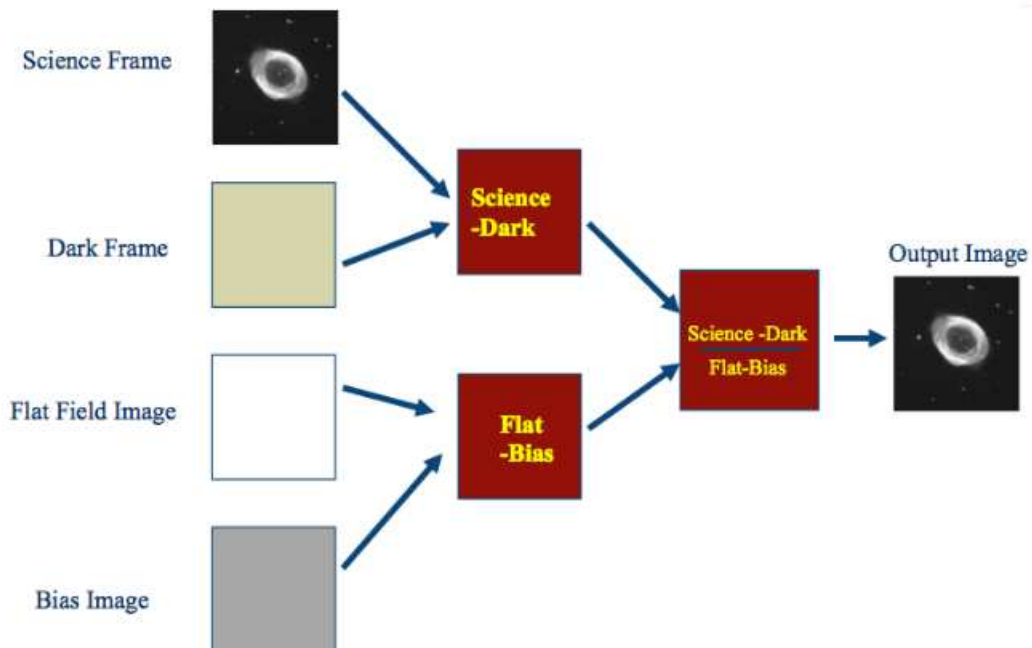


FIGURE 2.3: A simplified flow chart illustrating the basic data reduction process. As illustrated, dark frames (if necessary) are subtracted from a target frame, while the bias signal of the chip is subtracted off of the flat-field image. The quotient of the remaining science image and the perfect flat is taken to produce the output image, which will then be wavelength- and flux-calibrated.

2.4.2 Flat Preparation

To begin, contamination by other light sources and cosmic rays must be removed from the charge-coupled device (CCD) chip. This chip registers the refracted light coming through the long slit. Bias images are taken with nominal zero second exposures. Ten to twenty of these will normally be taken each night. An average is then taken to add to the “perfect flat” which is subtracted from each frame. In addition, sky flats are taken at twilight to account for atmospheric emission lines, and dome flats (flat-field frames) are taken with a quartz lamp. With sky and dome flats, it is crucial that the CCDs are not saturated, so that the relative intensities of the lines is maintained. On the DBS, the saturation limit was approximately 60,000 counts. An effort was made

to obtain an average of $\sim 30,000$ counts across the wavelength range.

Before preparing the perfect flat, we use the `findgain` task in IRAF to find the gain and readout noise for the CCD. This requires values for the useful x and y limits on the chip; we do this to exclude those portions of the chip that were not exposed to the observed object and lie on the “margins”.

Once we have the readout noise and the gain, we may insert these parameters into the `zerocombine.par` file and run to combine the bias flats. This process averages the values for each individual point across the several bias flats. A similar routine is followed with the sky flats and dome flats using the `flatcombine` package.

When this is done, we must use the `response` package to examine the dome flats. This package sums the pixel values along each column and outputs a curve representing the intensity of light along the dispersion axis. The quartz lamp is an incandescent bulb with a more or less constant energy output across the spectrum, so the `response` package allows us to determine how much light reaches each column along the dispersion axis. Knowing this, we can calibrate the object images such that the intensity of the columns, which each correspond to an individual wavelength, are adjusted to the levels we would see if the CCD were uniformly illuminated. The output file of `response` is typically called “nDOME”.

Turning now to the sky flats, we can subtract bias- and flat-field functions to produce “nSKY”. We do this using the `ccdproc` package in IRAF. We will then need to smooth the output’s low frequency variations in the `illumination` package, setting both the `high_rej` and `low_rej` parameters to 3 (the number of standard deviations). Pressing “Enter” at each bin fits that particular bin (the number of which can be changed in the parameter file) in a fashion similar to `response`. The order of the polynomial fit can be changed using `:on` (where n is the order), followed by “f”. We can then use the smoothed “nSKY”—renamed “ISKY”—to create the perfect flat using `imarith`. Multiplying the nDOME and ISKY flats, we arrive at the perfect flat.

2.4.3 Flat Subtraction

When we have obtained the perfect flat, we take a raw, unreduced CCD image, as seen in Figs. 2.4 and 2.5.

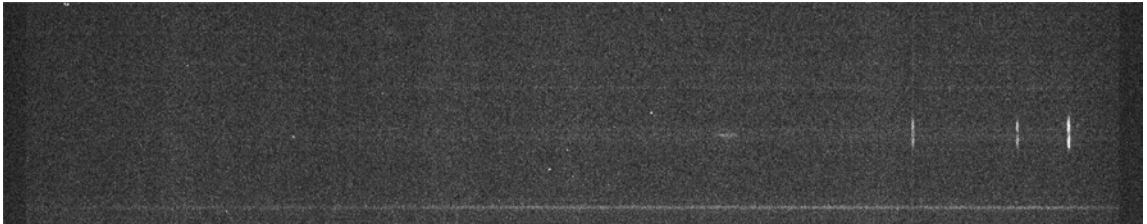


FIGURE 2.4: An image of the CCD chip after observing the planetary nebula Abell 48 through the blue arm of the 2.3 Metre Dual Beam Spectrograph. The spatial direction (the direction of the slit) is along the vertical axis, and the dispersion direction is along the horizontal axis. This observation was taken 11 May 2008.

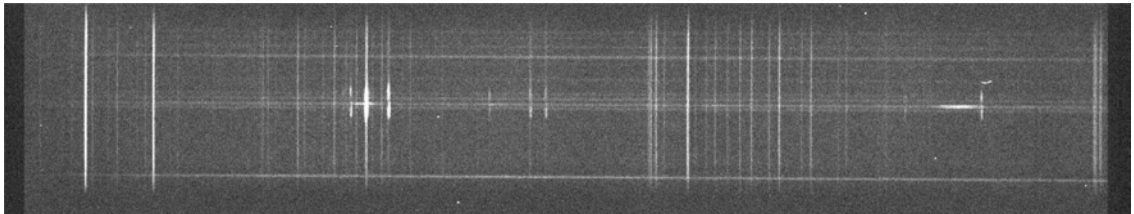


FIGURE 2.5: An image of the CCD chip after observing the planetary nebula Abell 48 through the red arm of the 2.3 Metre Dual Beam Spectrograph (DBS). As before, the spatial direction is along the vertical axis, and the dispersion direction is along the horizontal axis. This exposure was taken concurrently with the blue image on 11 May 2008.

We then use `ccdproc` to process all of the flats that need calibration. We do this by setting the “zero” parameter to our smoothed bias file and the flat to the perfect flat file.

2.4.4 Cosmic Ray Cleaning

For this task we used the `lacos_spec` package of the L.A. Cosmic software written by Pieter van Dokkum (van Dokkum 2001). This software causes the pixel image to be convolved with a Laplacian of a two-dimensional Gaussian of form

$$f(x, y) = \exp\left(-\frac{r^2}{2\sigma^2}\right) \quad (2.1)$$

where $r \equiv x^2 + y^2$ and σ represents the standard deviation. Because a cosmic ray has very sharp edges, its point spread function is not smooth. Thus, cosmic rays can be identified and removed. The number of iterations and order of the fitting function can be changed in the parameter file.

An example of a cosmic ray cleaned CCD is shown in Figure 2.6.

2.4.5 Spectrum Extraction

The next step is to bin the counts in the vertical (spatial) axis along a small strip of the horizontal (dispersion) axis of the CCD. Each strip naturally corresponds to a specific object on the slit. In the case of the data presented in this thesis, most of the relevant objects were planetary nebulae, and therefore strips both above and below the stellar lines must be combined to obtain the nebular spectra. Now we make use of PNDR (mentioned above). To use PNDR, it is necessary to create a data file denoting the vertical limits for the regions containing the sky, nebula, and stellar spectra, along with identifying information for the arc lamp exposures to be used. Once these numbers are in the correct format (detailed in the PNDR manual), we can use the `extractor` package to reduce the image. This package will produce individual “SKY”, “ARC”, “NEB” and “STAR” spectra.

After this extraction, the spectrum will be binned as counts per column. An example is shown in Figure 2.8.

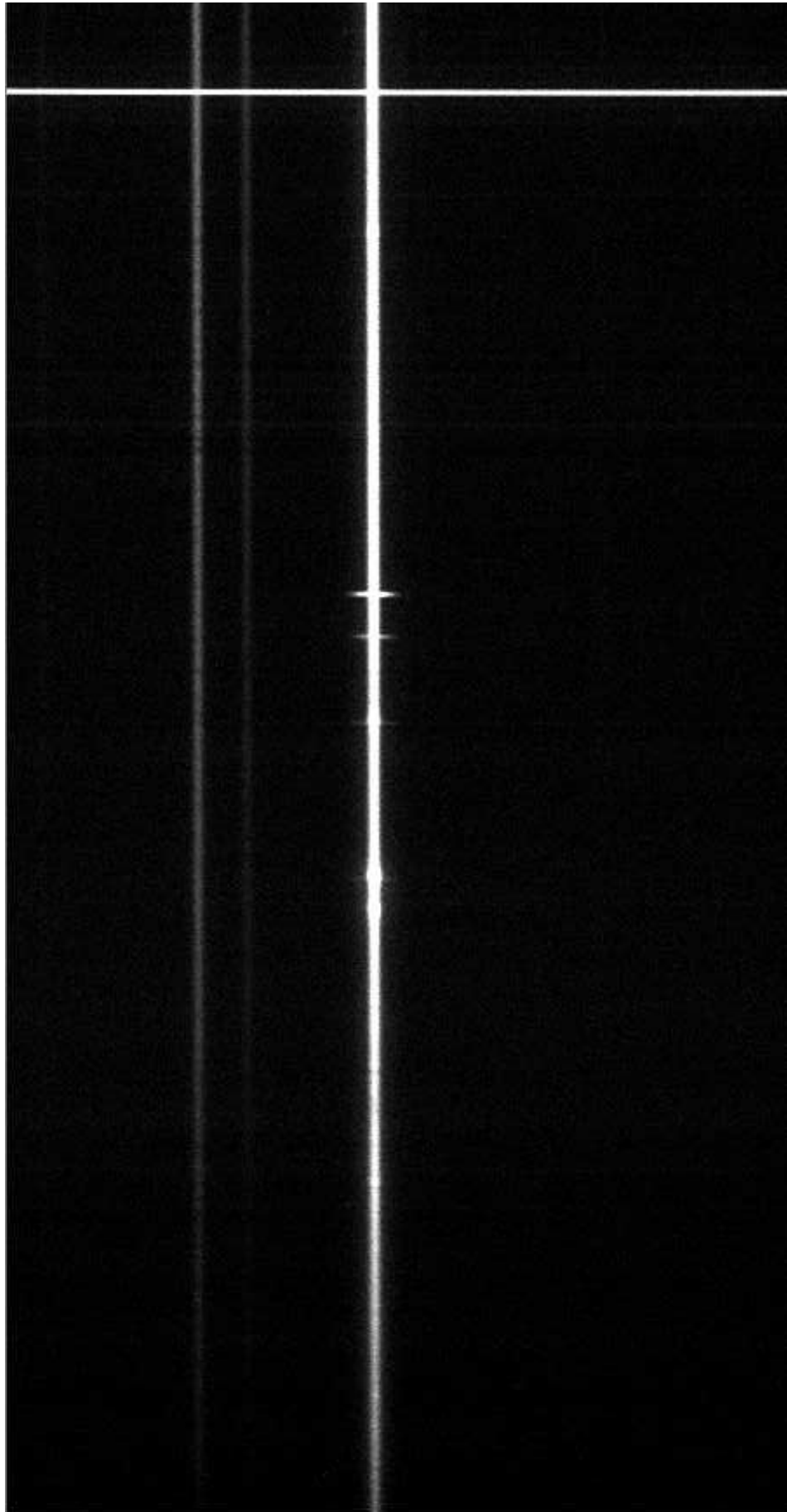


FIGURE 2.6: The previously presented spectrum after cosmic ray cleaning.

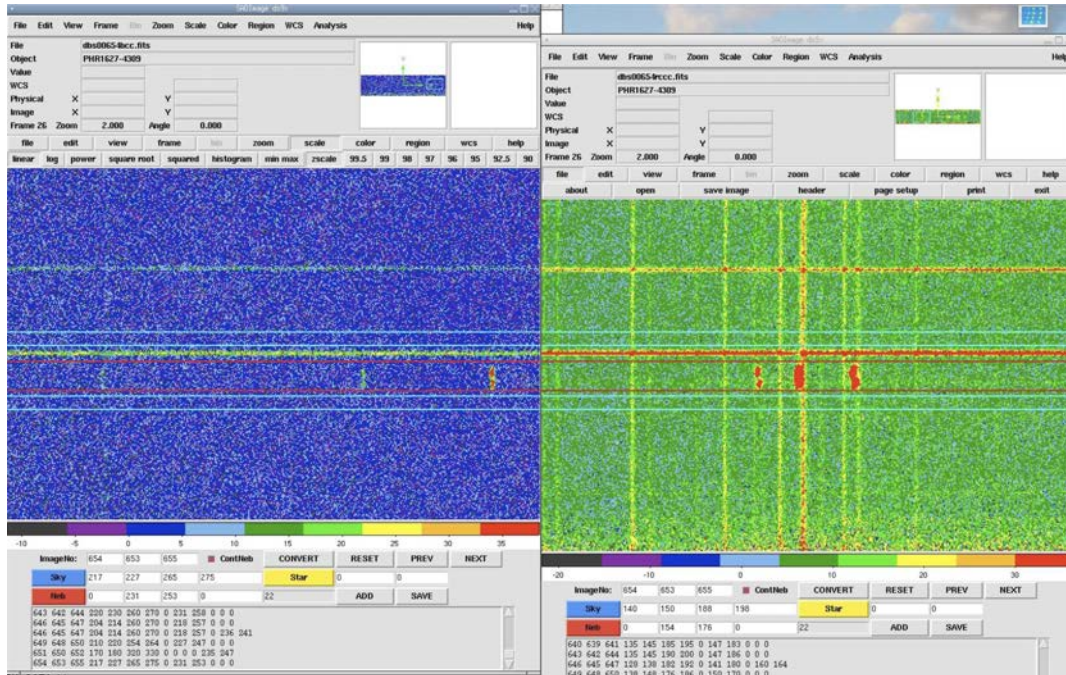


FIGURE 2.7: A screenshot of PDR. The horizontal lines represent the upper and lower bounds of regions on the plate which the user wishes to be binned. Separate regions are designated for sky (background) lines, for upper and lower nebular regions (either side of the star), and the star itself.

2.4.6 Wavelength Calibration

We now feed the list of arc images into a file (usually titled “arclist”). We then designate a file containing arc line information, e.g. `sso_cuhe.dat`. This file will serve as the “coordlist” in the `identify` and `reidentify` routines. We then choose one arc file and run `identify`. In some cases, the line list may not exist or the automatic line identification may not work properly. If this is the case, it may be necessary to identify the lines manually using an arc atlas. In this case, the user will be prompted to mark a certain number of lines using the “m” key and typing in the exact wavelength value for that position. Usually identifying 15 lines will enable a good fit. After running `identify`, we run `reidentify` using the original arc file as the reference image and process our arc list to calibrate all the arcs.

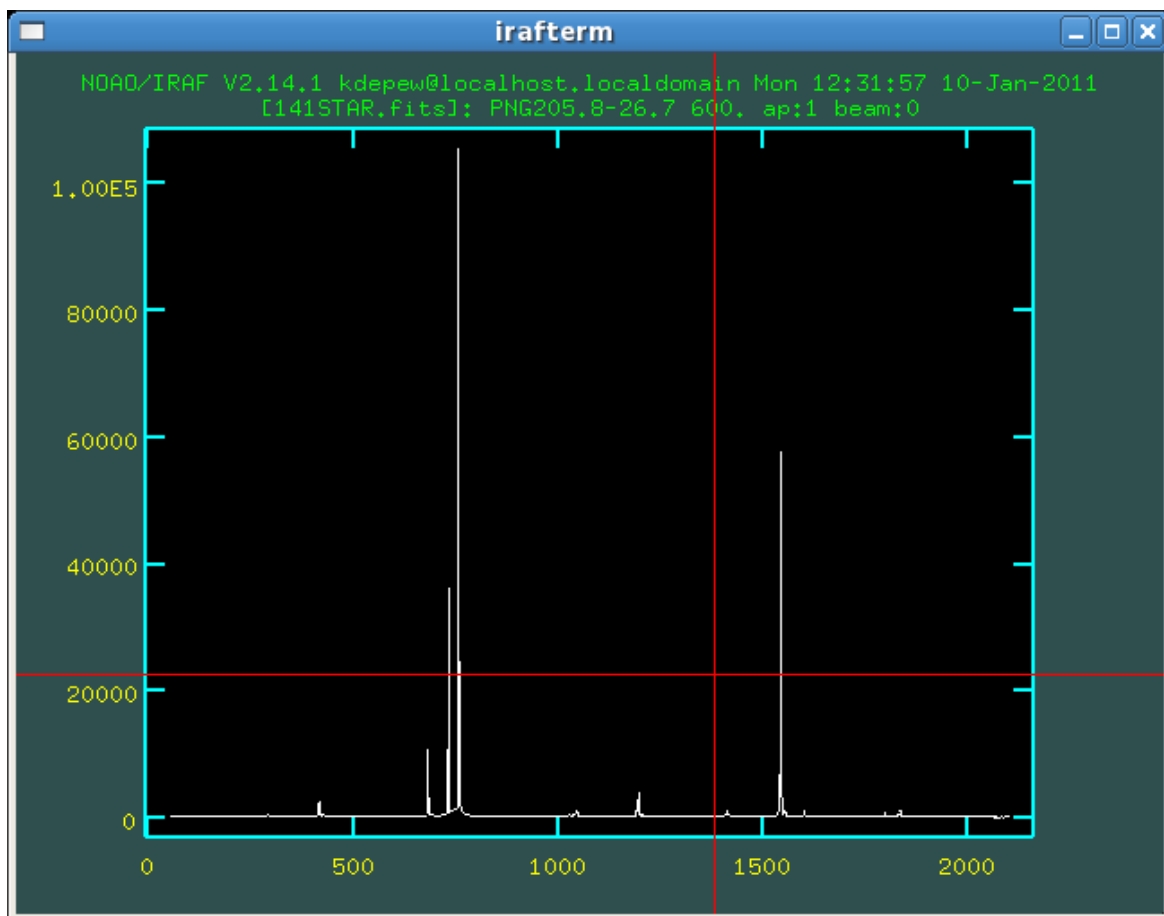


FIGURE 2.8: An example of a nebular spectrum awaiting wavelength- and flux-calibration.

We finally apply the dispersion solution obtained from `reidentify` to the object files by using the dispersion correction package `dispcor`. We now place all files we wish to calibrate into one list, usually labeled “`disp_in`”, and create a file called “`disp_out`” for the output.

2.4.7 Flux Calibration

In order to calibrate the flux levels, we now take the wavelength-calibrated spectrum of a spectrophotometric standard star that was observed at some point during the same night and a file containing extinction data for the observation site. This file uses the attenuation of radiation passing through the atmosphere as a function of wavelength

and airmass, as the name implies. We set the “extinct” parameter of the package `standard` to the name of this extinction file.

Moving on to the `caldir` package (located in `onedstds.ctiocal`), we set the observatory and the image file names in the parameter file. The name of the calibrating file in the IRAF directory will have a similar name to the object observed (e.g. `l6248` for `LTT6248`). This calibrating file indicates the exact flux value of each wavelength in the file. We then run `caldir`. Next we ensure that the “observat” parameter in the `sensfunc` package is set, and run it. This enables us to determine the sensitivity of the CCD as a function of wavelength.

Finally we create an input and output list of files to be acted upon by the `calibrate` package and run it. This will finish the flux-calibration of the data using IRAF.

2.5 WiFeS Data

The **Wide Field Spectrograph** (WiFeS) instrument was commissioned in March and April 2009 following the decommissioning of the DBS. The purpose of WiFeS is to enable three-dimensional spectra of objects to be taken. Unfortunately, at present, the full functionality is not available due to ongoing revisions and updates to the software. Therefore, the only available spectra are two-dimensional, similar to that which the DBS produced with long-slit observations. The primary advantage is the ability to select different regions of an object for data reduction, although absolute flux calibration is impossible for objects larger than the aperture (see Chapter 4).

WiFeS employs an image slicer (see Fig. 2.10) to split an image into 25 separate spectra for different portions of the object, allowing a three-dimensional data set.

The WiFeS data reduction package works within IRAF and requires `gemini` to be installed.

Grating	Ruling Density	Blaze Wavelength	R	Simultaneous Coverage	Wavelength Interval	Wavelength Offset	Y-offset
	lines/mm	μm		μm	nm	nm	pix
U7000	1948.0	0.3850	7000	0.109	0.329 - 0.438	0.0	0.0
B7000	1530.0	0.4900	7000	0.140	0.418 - 0.558	0.0	0.0
R7000	1210.0	0.6200	7000	0.177	0.529 - 0.706	0.0	0.0
I7000	937.0	0.8000	7000	0.229	0.683 - 0.910	0.0	0.0
B3000	708.0	0.4680	3000	0.270	0.320 - 0.590	0.0	0.0
R3000	398.0	0.7420	3000	0.450	0.530 - 0.980	0.0	0.0

FIGURE 2.9: The selection of gratings available on WiFeS. Taken from the the Australian National University WiFeS user pages (http://msowww.anu.edu.au/observing/ssowiki/index.php/WiFeS_Main_Page).

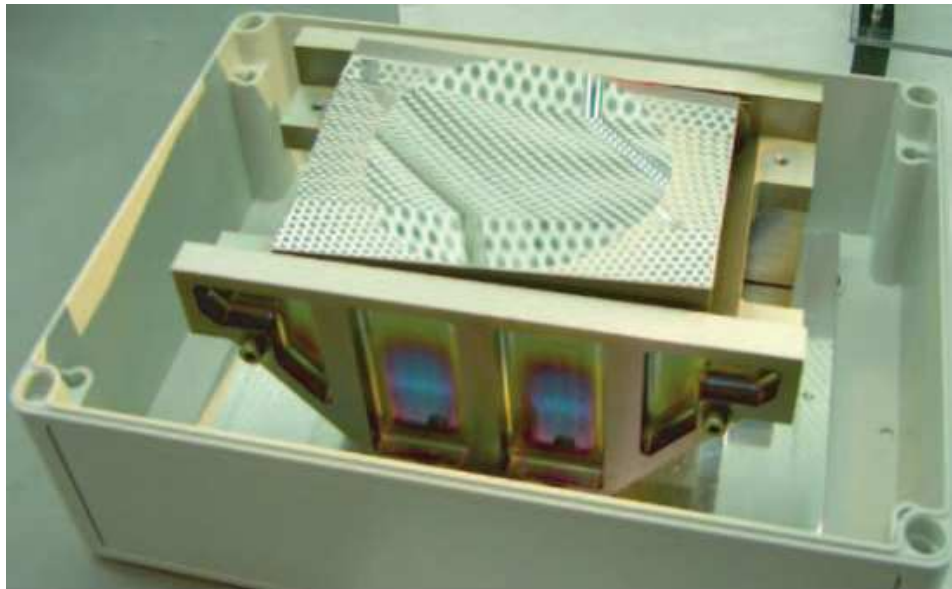


FIGURE 2.10: The image slicer of WiFeS, as shown in the observing manual, available at http://msowww.anu.edu.au/observing/ssowiki/index.php/WiFeS_Main_Page. Note the concentric design, which follows the same concepts as McGregor et al. (1999) and McGregor et al. (2003).

2.5.1 File Preparation

The WiFeS data reduction pipeline is intended to be highly automated. For this reason, the `wftable` routine was written. `wftable` must be run twice. The first time,

the “GRATINGB”, “GRATINGR” and “BEAMSPLT” parameters in the headers of the files to be reduced must be erased. After ensuring that `wftable` the grating and beamsplitter parameters are blank in `wftable.par`, `wftable` is run the first time. This process converts the FITS files to multi-extension FITS (MEF) files. This is necessary to permit the later production of a data cube using 25 image extensions.

Next, the appropriate grating is set in both the “GRATINGB” or “GRATINGR” parameters in the header files, as well as the `wftable.par` file (e.g. “B7000” for blue arm data obtained using the B7000 grating). We then insert the proper dichroic name for the “BEAMSPLT” parameter in the file headers and in `wftable.par`. After running `wftable` a second time, the routine will automatically produce lists of input files, divided according to the function of the file: object files, arc files, sky and dome flats, as well as bias (“zero”) exposures and “wire” flats—used for spatial alignment—are all assigned to a list.

2.5.2 Calibrations

The next package to be used is the `wfcal` routine. This step is optional, however; the WiFeS pipeline includes a set of calibration files which generally yield a better reduction than an average observer’s files, due to the number of exposures taken.

The `wfcal` package will automatically combine bias and flat files to subtract from the object file later on during the `wfreduce` routine. Because the file names are already divided up into sky files, arc files, etc., little input from the user is required. The user is required to approve fits of dome flats and arc files, but otherwise this process is accomplished entirely by the software. The reduced files will normally be placed in a file labeled “cal” or something similar within the data file directory.

2.5.3 Final Reduction

Finally, the `wfreduce` package must be opened. The parameters in `wfreduce.par` can be altered to designate the central wavelength (the image of the object in this wavelength is used to locate the desired aperture), whether user or pipeline calibration files will be used, etc.

This package will automatically subtract the sky flats and calibrate the images. The observer can then select a specific wavelength in which to view the object, which permits the selection of the relevant two-dimensional sky area which we wish to extract. See Figure 2.11 for an example.

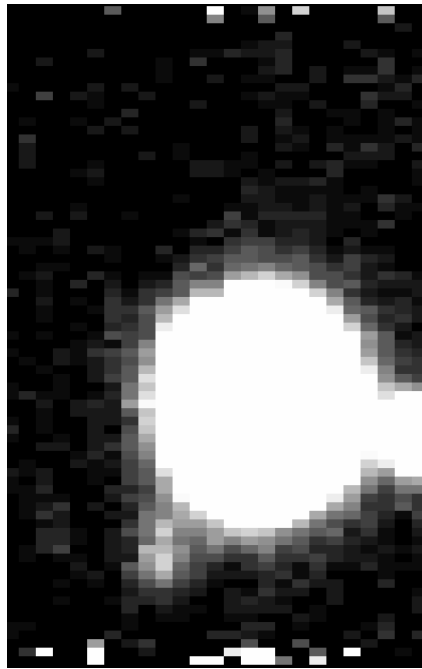


FIGURE 2.11: An image of the PN PB8 in $H\alpha$ after subtracting sky lines.

2.6 SPIRAL Data Reduction

Service observations on the Anglo-Australian Telescope (AAT)'s $AA\Omega$ spectrograph (see Figures 2.12 and 2.13). supplemented those taken on the 2.3 metre. During

these observations, the SPIRAL Integral Field Unit (IFU) was used. SPIRAL does not possess its own unique procedure for data reduction. Instead, it makes use of the Two-Degree Field Data Reduction (2dfdr) facility, which has been adapted for that purpose. Like the WiFeS reduction pipeline, it is highly automated. Links to data reduction manuals, signal-to-noise calculators, etc. can be found at http://www.aao.gov.au/AAO/2df/aaomega/aaomega_spiral_intro.html. Installation files may be downloaded from <ftp://ftp.aao.gov.au/pub/2df/>.

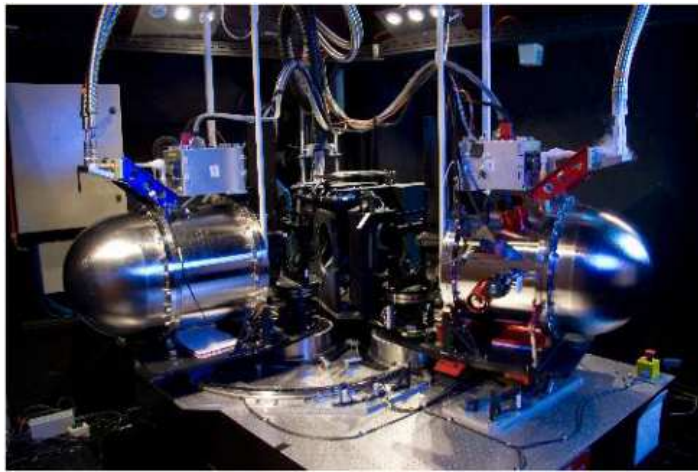


FIGURE 2.12: The AAOmega spectrograph.

The SPIRAL Integral Field Unit consists of an array of lenslets. These lenslets feed light into a 32×16 array of fibres (see Fig. 2.14). Each fibre is fed into the spectrograph, which results in 512 spectra. The IFU covers a rectangle of a 22×11 arcsecond area, and 0.7 arcsec pixels.

The 2dfdr software extracts spectra from images, then wavelength-calibrates, flat-fields, calibrates for throughput, and sky-subtracts the data.

2.6.1 Data Preparation

When beginning the data reduction process in 2dfdr, data files must be in NDF format—i.e. they must possess a “.sdf” file extension. If the files have been stored in a FITS

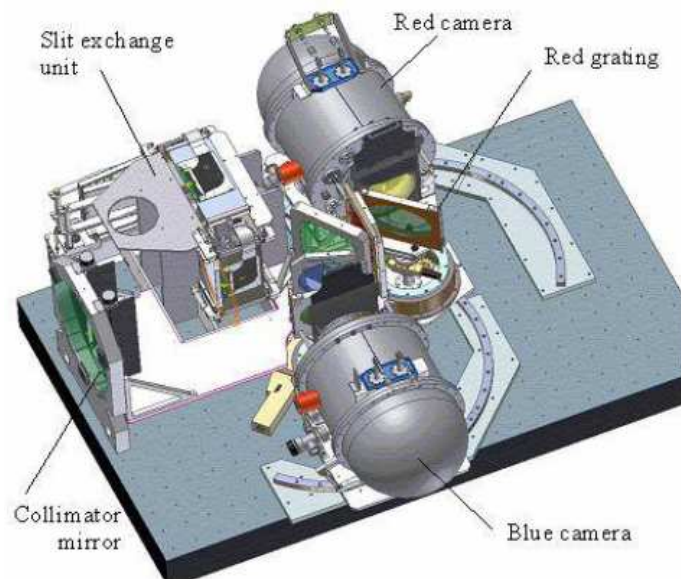


FIGURE 2.13: A schematic diagram of AAOmega, showing the red camera in high dispersion mode, and the blue camera in low dispersion mode.

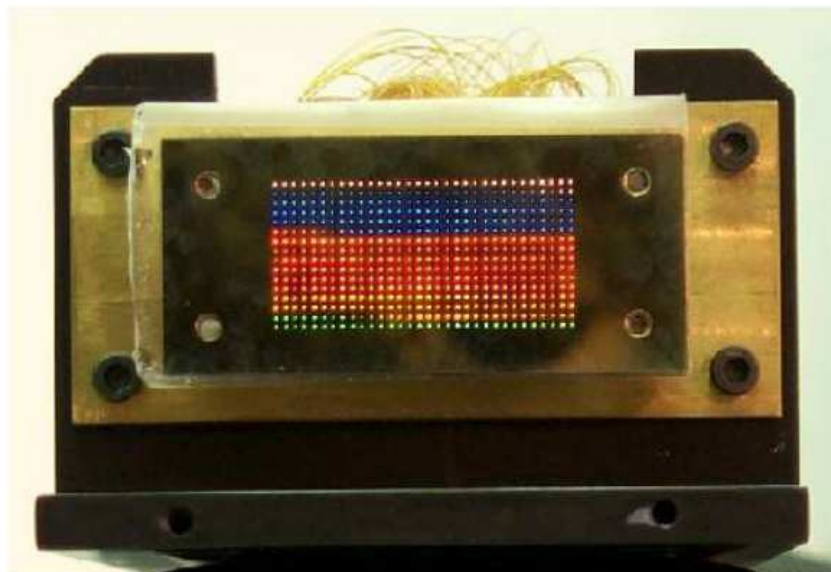


FIGURE 2.14: The SPIRAL IFU, which is designed for use with AAOmega. Its 32×16 array of fibres allows a possible 512 separate spectra.

format (as if often the case), they can be converted to NDF using the “fits2ndf” command.

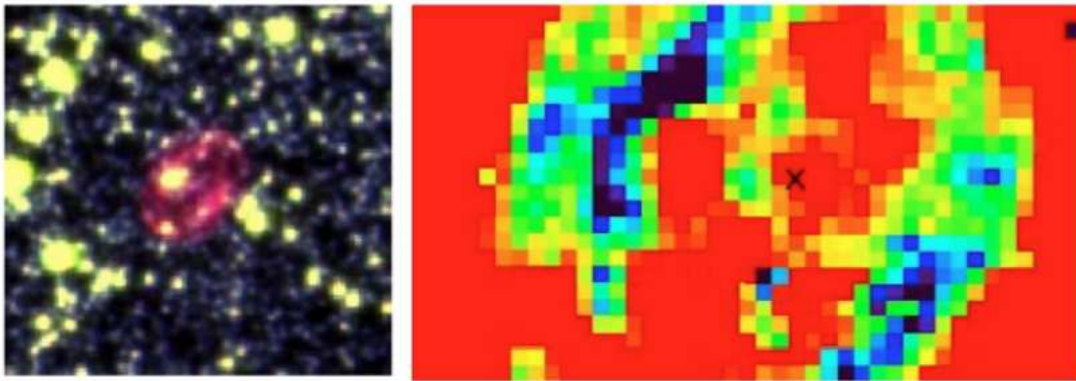


FIGURE 2.15: At left is a composite colour image of the MASH PN PHR1811-3042 (see Chapter 3) with $H\alpha$, short red and B band images represented as red, green and blue respectively, obtained from the online SuperCOSMOS survey data (Parker et al. 2005). At right is the same PN observed by SPIRAL at commissioning on 28 June 2006. Images taken from Sharp & The Aaomega+Spiral Team (2006a).

For SPIRAL data reduction, `2dfdr` requires one flat field taken with a quartz lamp in the chimney calibration unit. (This is necessary to locate fibres on the CCD.), at least one arc file, and of course the data files. Twilight or sky flats are optional. All files taken with the same grating and central wavelength should be placed in the same directory. All files should have the `INSTRUME` keyword in the FITS file header set to “Spiral” in order for `2dfdr` to properly recognize them.

The `2dfdr` is then launched using the “`drcontrol spiral.idx &`” command. An interface should appear as shown in Figure 2.16.

The user should make sure that all files are correctly classified. To do this, the user must select “Set Class...” from the “Commands” menu, select the file, and specify a class for it. If a file is taken from an object, the class should be set as “MFOBJECT”. Likewise, the class should be set as “MFFF” for flat fields, “MFARC” for arc files, and “MFSKY” for the twilight flats.

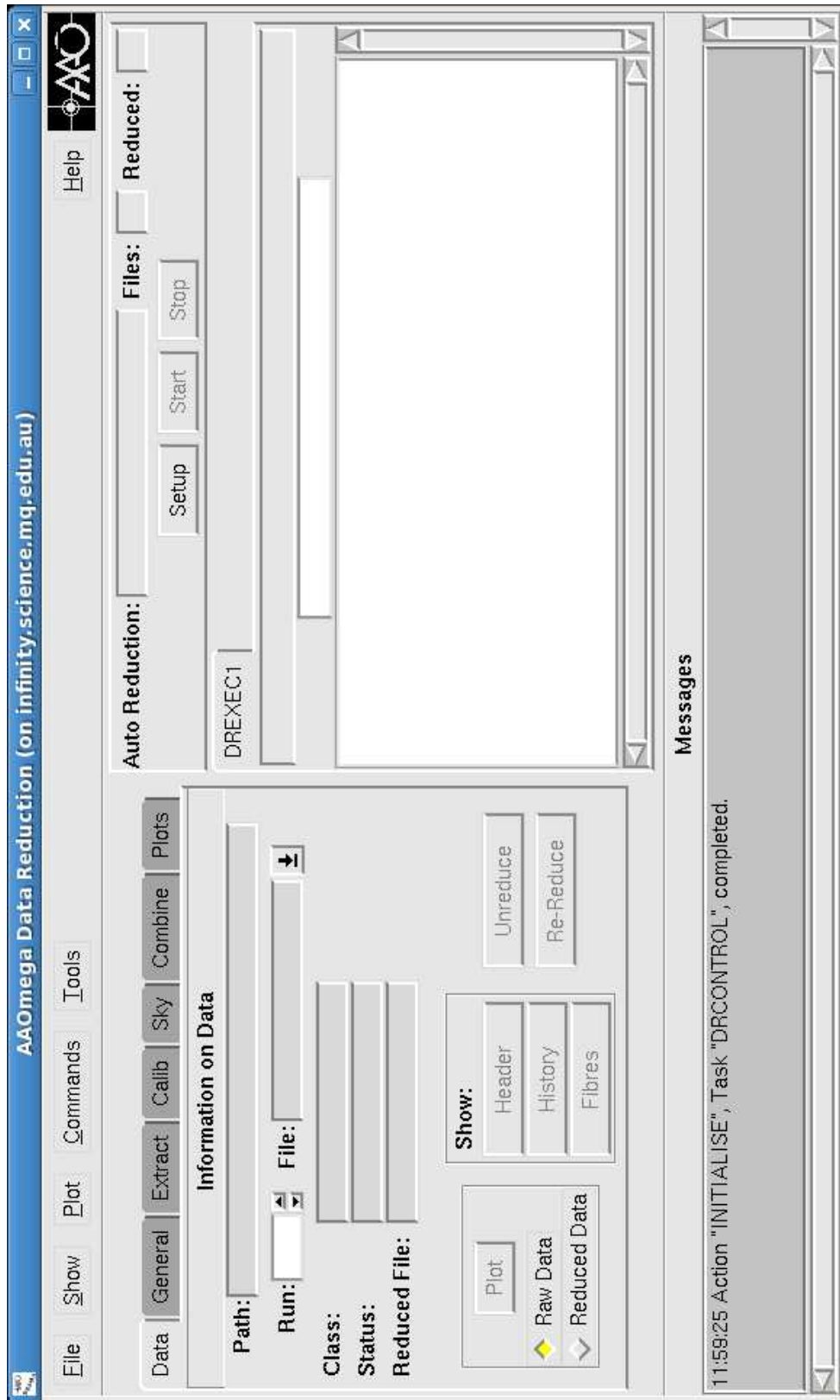


FIGURE 2.16: The 2dfdr data reduction facility interface.

2.6.2 Data Reduction

The 2dfdr facility was designed to be essentially automatic if all files are properly identified and ordered. However, one further file is required: the spiral.dat file. A default version should be available from the download directory. The spiral.dat file provides the reduction software with information on which fibres in the AA Ω spectrograph are functional, as well as the number of grating lines per millimetre, central wavelength in angstroms, and the name of the calibration lamp used.

The next step is to produce a tram-line map. To do this, we choose “REDUCE” from the “Commands” menu and select a flat field file. The tram-line map will then be created by taking a cut down the centre of the flat field image and finding the individual peaks, which correspond to the individual spectrograph fibres. This allows the program to make a rotation adjustment of the data later on. Curvature, which is due to distortion in the optics of the spectrograph, is fitted to a radial distortion model.

While theoretically 512 peaks should be found in the tram-line map, three fibres are never useable; one is broken and two are too close to neighbouring fibres to be able to differentiate between them. Thus, only around 509 peaks are generally found. If the number is much less than 500, the focus is probably poor and the spectrograph should be refocused.

After the tram-line map has been produced, the user selects “Plot Tram Map...” from the “Commands” menu. After choosing the appropriate “tln” file, the tram-line map is plotted and the number of fibres that were found can be counted. If for any reason the number of fibres listed in the spiral.dat file is different from that found by the reduction software, the spiral.dat file must be altered such that the non-existent line is commented out. The procedure is then rerun until the spiral.dat file is in agreement with the image.

After the tram-line map is reduced, the “Rotate/Shift to Match” option on the

“Extract” parameters page is switched to “OFF” and the other flat fields are then reduced.

At this point it is usually possible to set the reduction facility to its automatic mode, but the further steps will be described below for the manual case.

Arc Reduction

Arc reduction follows a similar process: the “Reduce” option in the “Commands” menu is selected, and an arc lamp exposure is chosen. The software automatically aligns the columns according to the tram-line map and, provided that the right arc lamp code is entered into the directory’s spiral.dat file, it should correctly identify the strongest lines.

Twilight Flat Reduction

Again, twilight flats are chosen using the “Reduce” option in order to calibrate relative fibre throughput. If more than one sky file is present, these will be automatically combined and the throughput will be calibrated according to the combination.

Object Data Reduction

When selecting object images for reduction, the “General” parameters page allows the user to choose whether or not he/she wishes to use 1) flat-fielding from a fibre flat, 2) throughput calibration from sky lines, and 3) sky subtraction.

The same “Reduce” option is employed with the object files. If desired, reduced runs can then be combined using the “Combine Reduced Runs...” option in the “Commands” menu. This method will automatically reject cosmic rays. However, high S/N data may necessitate an increase in the “Rejection Threshold” parameter.

The resulting reductions can be plotted by selecting “Plot” in the “Commands” menu. To condense spectra into one dimension, the IRAF routine `imcombine` may be

used:

```
iraf> imcombine image.fits[0] reject=none combine=sum proj=yes
```

Chapters 3-6 (pp. 63-198) have been omitted from this thesis for copyright reasons.

Chapter 3 has been published as a journal article. Please refer to the following link for the abstract details.

DePew, K., Parker, Q.A., Miszalski, B., De Marco, O., Frew, D.J., Acker, A., Kovacevic, A.V. & Sharp, R.G., (2011), Newly discovered Wolf-Rayet and weak emission-line central stars of planetary nebulae, *Monthly notices of the Royal Astronomical Society* 414(4), pp. 2812-2827.

<http://dx.doi.org/10.1111/j.1365-2966.2011.18337.x>

7

Conclusions

*The disciples said to Jesus, “Tell us how our end will be.” Jesus said,
“Have you discovered the beginning then, that you look for the end?”*

—The Gospel of Thomas, Verse 18

Overview

Approximately 97% of intermediate-mass ($0.8-8M_{\odot}$) stars will pass through a PN stage. Stars that eventually develop into [WR] CSPNe, comprising somewhere between 7 and 9% of all CSPNe, therefore represent a significant portion of the Galactic stellar

population. By understanding the mechanisms that lead to H-deficiency, we may shed some light on late stellar evolution as a whole. In the course of this thesis, I have attempted to make some contribution to the understanding of this area.

7.1 The [WR] Population

The MASH survey has made a large contribution to the list of known [WR] stars, increasing the sample by $\sim 30\%$. It is evident from this number that the Wolf-Rayet phenomenon is by no means rare; these objects appear to form a regular component of the local neighbourhood and possibly the universe as a whole.

I have detailed a number of new [WR] and WELS discoveries, most notably:

- 22 previously unpublished [WR]s found in both the MASH sample and in the population of known Wolf-Rayets and

- 10 previously unpublished WELS identifications.

Attempts at classification have been made according to both the most widespread classification schemes, i.e. that of Crowther et al. (1998) and Acker & Neiner (2003).

- The 22 new [WR]s increase the known [WR] sample by over 27%.

- The new WELS increase the number of known WELS by over 11%.

7.2 The [WN/WC] Stars

The existence of a nitrogen-rich [WR] sequence is still controversial. It is possible, considering the evidence presented in this thesis, that pure [WN] stars may not exist, but may be misidentifications of other objects, notably massive WN stars or accreting

white dwarfs. However, it seems likely that there does indeed exist a [WN/WC] class comprised (at present) of the central stars of PB 8 and Abell 48. The PN status of both of these enigmatic objects is widely accepted, but it is still unknown why these stars exhibit nitrogen-enriched matter at their surfaces when the surrounding nebula is not Type I. Major points include:

- The PNe surrounding PB 8 and Abell 48 appear to be quite similar, albeit Abell 48 likely has higher metal enrichment than indicated by the modeling presented in this thesis, owing to the shallow nature of the nebular spectrum we have obtained. PB 8 is not a Type I PN, and Abell 48 is unlikely to be either. Both appear to be classed as WN6 according to the scheme of Conti et al. (1990). PB 8 is classed as a [WN6/WC7], while Abell 48 appears to be a [WN6/WC5-6].

- Both PNe appear to have multiple faint rings that were not previously described but are visible in $H\alpha$ /SR quotient images. This may suggest similar life histories, with these (probably older) arcs possibly indicating past pulsations and mass-loss.

- Both PNe have similar dynamical ages. While the kinematic structure of Abell 48 is complicated by its multiple rings, if we assume an average [WR] v_{exp} of 36 km s^{-1} (Peña et al. 2003b) and take the distance of 1.2 kpc derived from the SB-r relation in Frew (2008), we obtain a dynamical age of a little over 3500 years. This compares to a dynamical age of 2700 years for PB 8. This indicates that the [WN/WC] phase, when it does occur, may occupy a specific period in the lifetime of a star.

- Owing to its rarity and youth, the [WN/WC] class likely represents a transitory phase. However, more specimens should be found and modeled before any firm conclusions are drawn.

7.3 The Subclass Evolutionary Sequence

The work presented here suggests that late [WC] types probably evolve into the early [WC]s and [WO]s. Evidence from dynamical age, excitation class, and effective temperature determinations bolster this assumption. As it currently stands, the dearth of Galactic [WC6-9] types appears to be the result of a very fast evolution of [WC]s across this gap, on the order of perhaps 1000 years or less.

7.4 The Evolutionary Relationship Between [WR]s, WELS and PG1159 Stars

Previous studies of [WR]s and WELS have focused on studies of surface temperature, terminal wind velocity, etc. in an attempt to determine the evolutionary relationship, if any, between these two groups. Other scenarios which place the WELS into the [WC5-7] gap may at first appear to be reasonable. However, as shown in Chapter 6, WELS possess a much larger average Galactic height, suggesting that they descend from lower metallicity, lower mass progenitors. The WELS are not entirely restricted to higher $|z|$, however, and it remains to be seen whether this larger spread in metallicities points to a heterogeneous origin for these objects.

The PG 1159 stars exhibit a height distribution similar to that of the WELS. At the least, we can say that the [WR] stars, with their tight concentration at lower $|z|$, probably do not evolve into PG1159 stars, or are in any case not responsible for the entire class. The PG1159 stars should be expected to have lower progenitor masses and lower abundances of heavy elements. The question of what the [WR]s evolve into later on is an important question. It may be true that both [WR]s and WELS evolve into this one class, but if this were true, considering the number of known [WR]s, the PG1159s would likely cluster more strongly at lower $|z|$, as well as at WELS $|z|$ heights.

7.5 Future Work

Deep, high-quality spectra are crucial to continue any investigation into the evolution of H-deficient CSPNe. There is great potential for misclassification due to “missing” lines. Some [WR] spectra exhibiting a C IV $\lambda\lambda 5801,12$ doublet may also possess a weak C III $\lambda 5696$ component. Unless the continuum is detected in these faint objects, it is possible that an observer may classify an early-type [WR] as a WELS. In addition, if deep blue spectra are not obtained, the 4650\AA WELS complex could be entirely overlooked, leading to the classification of a WELS as a [WR]. A committed effort to re-examine the spectra of [WR]s and WELS may result in a significant rearrangement of class membership. However, because such deep spectra are required for over 200 objects, a large amount of observing time is required simply for this proposed verification.

A re-examination of the known [WR]s, carried out with deep spectra, may reveal more examples of [WN/WC] subtypes. Considering that the central stars of PB 8 and A 48 are so similar, possessing the same temperature and spectral characteristics, comparison of [WC5-6] and [WN/WC] chemical models would be very valuable. There may be a specific abundance profile that leads to this subclass.

A larger set of dynamical ages, especially for the little-represented [WC5-7] “gap” subclasses, should be obtained. The limiting factor here is the spectral resolution available on a given observation instrument. Spectral resolution of greater than $\sim 10,000$ is required to measure the nebular expansion velocities precisely. Nebular expansion velocities are lacking in the literature—especially for the newly discovered [WR]s and WELS found in the MASH sample—and more [N II] velocities should be measured where available. This will allow us to fill in more points on the subclass-dynamical age chart, which is unfortunately sparse in the region of the late [WC]s and the “gap” objects between [WC5] and [WC7] subtypes.

The chemical abundance modeling of more [WR]s, WELS and PG1159s should be

undertaken, without any assumption that these three classes are related. It is also possible that there may exist degeneracies in the chemical composition of these stars that could lead to the same spectral type.

References

- Abbott, D. C., & Conti, P. S. 1987, *ARA&A*, 25, 113
- Abell, G. O. 1955, *PASP*, 67, 258
- . 1966, *ApJ*, 144, 259
- Acker, A., Gesicki, K., Grosdidier, Y., & Durand, S. 2002, *A&A*, 384, 620
- Acker, A., Marcout, J., Ochsenbein, F., Stenholm, B., & Tylenda, R. 1992, *Strasbourg - ESO catalogue of galactic planetary nebulae. Part 1; Part 2*, ed. Acker, A., Marcout, J., Ochsenbein, F., Stenholm, B., & Tylenda, R.
- Acker, A., & Neiner, C. 2003, *A&A*, 403, 659
- Akashi, M., Soker, N., & Behar, E. 2006, *ApJ*, 644, 451
- Aller, L. H. 1956, *Gaseous nebulae*, ed. Aller, L. H.
- Althaus, L. G., Panei, J. A., Miller Bertolami, M. M., García-Berro, E., Córscico, A. H., Romero, A. D., Kepler, S. O., & Rohrmann, R. D. 2009, *ApJ*, 704, 1605
- Althaus, L. G., Serenelli, A. M., Panei, J. A., Córscico, A. H., García-Berro, E., & Scóccola, C. G. 2005, *A&A*, 435, 631

- Balick, B., Perinotto, M., Maccioni, A., Terzian, Y., & Hajian, A. 1994, *ApJ*, 424, 800
- Boffi, F. R., & Stanghellini, L. 1994, *A&A*, 284, 248
- Bohannon, B., & Walborn, N. R. 1989, *PASP*, 101, 520
- Bond, H. E. 2010, in *American Institute of Physics Conference Series*, Vol. 1273, American Institute of Physics Conference Series, ed. K. Werner & T. Rauch, 225–230
- Bond, H. E., & Ciardullo, R. 1999, *PASP*, 111, 217
- Boothroyd, A. I., Sackmann, I., & Wasserburg, G. J. 1995, *ApJ*, 442, L21
- Cahn, J. H., & Kaler, J. B. 1971, *ApJS*, 22, 319
- Cahn, J. H., Kaler, J. B., & Stanghellini, L. 1992, *A&AS*, 94, 399
- Calvet, N., & Peimbert, M. 1983, *RMxAA*, 5, 319
- Cardelli, J. A., Clayton, G. C., & Mathis, J. S. 1989, *ApJ*, 345, 245
- Charbonnel, C., & Zahn, J.-P. 2007, *A&A*, 467, L15
- Chesneau, O., et al. 2009, *A&A*, 493, L17
- Chiappini, C., Górný, S. K., Stasińska, G., & Barbuy, B. 2009, *A&A*, 494, 591
- Chu, Y., Treffers, R. R., & Kwitter, K. B. 1983, *ApJS*, 53, 937
- Chu, Y., Weis, K., & Garnett, D. R. 1999, *AJ*, 117, 1433
- Ciardullo, R., Bond, H. E., Sipior, M. S., Fullton, L. K., Zhang, C., & Schaefer, K. G. 1999, *AJ*, 118, 488
- Ciardullo, R., Sigurdsson, S., Feldmeier, J. J., & Jacoby, G. H. 2005, *ApJ*, 629, 499
- Clayton, G. C., & De Marco, O. 1997, *AJ*, 114, 2679

- Cohen, M. 1999, in *Astronomical Society of the Pacific Conference Series*, Vol. 168, *New Perspectives on the Interstellar Medium*, ed. A. R. Taylor, T. L. Landecker, & G. Joncas, 97
- Cohen, M., Parker, Q. A., Green, A. J., Miszalski, B., Frew, D. J., & Murphy, T. 2010, ArXiv e-prints
- Condon, J. J., & Kaplan, D. L. 1998, *ApJS*, 117, 361
- Condon, J. J., Kaplan, D. L., & Terzian, Y. 1999, *ApJS*, 123, 219
- Conti, P. S. 1976, *Memoires of the Societe Royale des Sciences de Liege*, 9, 193
- Conti, P. S., & Massey, P. 1989, *ApJ*, 337, 251
- Conti, P. S., Massey, P., & Vreux, J. 1990, *ApJ*, 354, 359
- Corradi, R. L. M., & Schwarz, H. E. 1995, *A&A*, 293, 871
- Corradi, R. L. M., et al. 2011, *MNRAS*, 410, 1349
- Córsico, A. H., Althaus, L. G., Miller Bertolami, M. M., & Werner, K. 2007, *A&A*, 461, 1095
- Crowther, P. A. 2000, *A&A*, 356, 191
- . 2007, *ARA&A*, 45, 177
- Crowther, P. A. 2008, in *Astronomical Society of the Pacific Conference Series*, Vol. 391, *Hydrogen-Deficient Stars*, ed. A. Werner & T. Rauch, 83
- Crowther, P. A., Abbott, J. B., Hillier, D. J., & De Marco, O. 2003, in *IAU Symposium*, Vol. 209, *Planetary Nebulae: Their Evolution and Role in the Universe*, ed. S. Kwok, M. Dopita, & R. Sutherland, 243
- Crowther, P. A., De Marco, O., & Barlow, M. J. 1998, *MNRAS*, 296, 367

- Crowther, P. A., Dessart, L., Hillier, D. J., Abbott, J. B., & Fullerton, A. W. 2002, *A&A*, 392, 653
- Crowther, P. A., Morris, P. W., & Smith, J. D. 2006, *ApJ*, 636, 1033
- Crowther, P. A., & Smith, L. J. 1997, *A&A*, 320, 500
- Crowther, P. A., Smith, L. J., & Hillier, D. J. 1995a, *A&A*, 302, 457
- Crowther, P. A., Smith, L. J., & Hillier, D. J. 1995b, in *IAU Symposium*, Vol. 163, *Wolf-Rayet Stars: Binaries; Colliding Winds; Evolution*, ed. K. A. van der Hucht & P. M. Williams, 147
- Crowther, P. A., Smith, L. J., Hillier, D. J., & Schmutz, W. 1995c, *A&A*, 293, 427
- Cuisinier, F., Acker, A., & Koeppen, J. 1996, *A&A*, 307, 215
- Davies, R. D., Elliott, K. H., & Meaburn, J. 1976, *MmRAS*, 81, 89
- De Marco, O. 2008, in *Astronomical Society of the Pacific Conference Series*, Vol. 391, *Hydrogen-Deficient Stars*, ed. A. Werner & T. Rauch, 209
- De Marco, O., & Barlow, M. J. 2001, *Ap&SS*, 275, 53
- De Marco, O., Barlow, M. J., & Storey, P. J. 1997, *MNRAS*, 292, 86
- De Marco, O., & Crowther, P. A. 1999, *MNRAS*, 306, 931
- De Marco, O., Crowther, P. A., Barlow, M. J., Clayton, G. C., & de Koter, A. 2001, *MNRAS*, 328, 527
- De Marco, O., Hillwig, T. C., & Smith, A. J. 2008, *AJ*, 136, 323
- De Marco, O., & Soker, N. 2002, *PASP*, 114, 602
- DePew, K., Parker, Q. A., Miszalski, B., De Marco, O., Frew, D. J., Acker, A., Kovacevic, A. V., & Sharp, R. G. 2011, *ArXiv e-prints*

- Dopita, M., et al. 2010, *Ap&SS*, 327, 245
- Dopita, M. A., & Evans, I. N. 1986, *ApJ*, 307, 431
- Dopita, M. A., Ford, H. C., & Webster, B. L. 1985, *ApJ*, 297, 593
- Dopita, M. A., & Hua, C. T. 1997, *ApJS*, 108, 515
- Dopita, M. A., & Meatheringham, S. J. 1990, *ApJ*, 357, 140
- Downes, R. A. 1984, *PASP*, 96, 807
- Dreizler, S., & Werner, K. 1996, *A&A*, 314, 217
- Drew, J. E., et al. 2005, *MNRAS*, 362, 753
- Eggen, O. J., Lynden-Bell, D., & Sandage, A. R. 1962, *ApJ*, 136, 748
- Eggleton, P. P., Dearborn, D. S. P., & Lattanzio, J. C. 2008, *ApJ*, 677, 581
- Eldridge, J. J., & Vink, J. S. 2006, *A&A*, 452, 295
- English, J., et al. 1998, *PASA*, 15, 56
- Epchtein, N., et al. 1994, *Ap&SS*, 217, 3
- Evans, I. N., & Dopita, M. A. 1985, *ApJS*, 58, 125
- Faundez-Abans, M., & Maciel, W. J. 1987, *A&A*, 183, 324
- Feast, M. W. 1968, *MNRAS*, 140, 345
- Ferguson, D. H., Liebert, J., Cutri, R., Green, R. F., Willner, S. P., Steiner, J. E., & Tokarz, S. 1987, *ApJ*, 316, 399
- Fogel, J., De Marco, O., & Jacoby, G. 2003, in *IAU Symposium*, Vol. 209, Planetary Nebulae: Their Evolution and Role in the Universe, ed. S. Kwok, M. Dopita, & R. Sutherland, 235

- Frew, D. J. 2008, PhD thesis, Department of Physics, Macquarie University, NSW 2109, Australia
- Frew, D. J., & Parker, Q. A. 2006, in IAU Symposium, Vol. 234, Planetary Nebulae in our Galaxy and Beyond, ed. M. J. Barlow & R. H. Méndez, 49–54
- Frew, D. J., & Parker, Q. A. 2010a, ArXiv e-prints
- . 2010b, PASA, 27, 129
- Frew, D. J., Parker, Q. A., & Russeil, D. 2006, MNRAS, 372, 1081
- Gamow, G. 1943, ApJ, 98, 500
- Garcia-Lario, P., Manchado, A., Suso, S. R., Pottasch, S. R., & Olling, R. 1990, A&AS, 82, 497
- García-Rojas, J., Peña, M., & Peimbert, A. 2009, A&A, 496, 139
- Gathier, R., Pottasch, S. R., & Goss, W. M. 1986, A&A, 157, 191
- Gaustad, J. E., McCullough, P. R., Rosing, W., & Van Buren, D. 2001, PASP, 113, 1326
- Gesicki, K., & Zijlstra, A. A. 2000, A&A, 358, 1058
- Gesicki, K., Zijlstra, A. A., Acker, A., Górny, S. K., Gozdziwski, K., & Walsh, J. R. 2006, A&A, 451, 925
- Girard, P., Köppen, J., & Acker, A. 2007, A&A, 463, 265
- Górny, S. K., Chiappini, C., Stasińska, G., & Cuisinier, F. 2009, A&A, 500, 1089
- Górny, S. K., & Siódmiak, N. 2003, in IAU Symposium, Vol. 209, Planetary Nebulae: Their Evolution and Role in the Universe, ed. S. Kwok, M. Dopita, & R. Sutherland, 43

- Górny, S. K., Stasińska, G., Escudero, A. V., & Costa, R. D. D. 2004, *A&A*, 427, 231
- Górny, S. K., Stasińska, G., Szczerba, R., & Tyllenda, R. 2001, *A&A*, 377, 1007
- Górny, S. K., & Tyllenda, R. 2000, *A&A*, 362, 1008
- Green, D. A. 1999, in *Astronomical Society of the Pacific Conference Series*, Vol. 168, *New Perspectives on the Interstellar Medium*, ed. A. R. Taylor, T. L. Landecker, & G. Joncas, 31
- Greiner, J. 2000, *New Astronomy*, 5, 137
- Gurzadian, G. A. 1988, *Ap&SS*, 149, 343
- Gurzadian, G. A., & Egikian, A. G. 1991, *Ap&SS*, 181, 73
- Gvaramadze, V. V., et al. 2009, *MNRAS*, 400, 524
- Hadfield, L. J., Crowther, P. A., Schild, H., & Schmutz, W. 2005, *A&A*, 439, 265
- Hajduk, M., Zijlstra, A. A., & Gesicki, K. 2010, *MNRAS*, 406, 626
- Hajian, A. R. 2006, in *IAU Symposium*, Vol. 234, *Planetary Nebulae in our Galaxy and Beyond*, ed. M. J. Barlow & R. H. Méndez, 41–48
- Hamann, W., Gräfener, G., & Liermann, A. 2006, *A&A*, 457, 1015
- Hamann, W., Peña, M., & Graefener, G. 2005, in *Astronomical Society of the Pacific Conference Series*, Vol. 334, *14th European Workshop on White Dwarfs*, ed. D. Koester & S. Moehler, 345
- Hamann, W., Peña, M., Gräfener, G., & Ruiz, M. T. 2003, *A&A*, 409, 969
- Hambly, N. C., Irwin, M. J., & MacGillivray, H. T. 2001, *MNRAS*, 326, 1295
- Harries, T. J., Hillier, D. J., & Howarth, I. D. 1998, *MNRAS*, 296, 1072

- Harris, H. C., et al. 2007, *AJ*, 133, 631
- Herwig, F. 2001, *Ap&SS*, 275, 15
- . 2005, *ARA&A*, 43, 435
- Herwig, F., Blöcker, T., Langer, N., & Driebe, T. 1999, *A&A*, 349, L5
- Heyer, M. H. 1999, in *Astronomical Society of the Pacific Conference Series*, Vol. 168, *New Perspectives on the Interstellar Medium*, ed. A. R. Taylor, T. L. Landecker, & G. Joncas, 54
- Higgs, L. A. 1999, in *Astronomical Society of the Pacific Conference Series*, Vol. 168, *New Perspectives on the Interstellar Medium*, ed. A. R. Taylor, T. L. Landecker, & G. Joncas, 15
- Hilditch, R. W., Harries, T. J., & Hill, G. 1996, *MNRAS*, 279, 1380
- Hillier, D. J. 1987, *ApJS*, 63, 947
- . 1988, *ApJ*, 327, 822
- . 1989, *ApJ*, 347, 392
- Hillier, D. J., Lanz, T., Heap, S. R., Hubeny, I., Smith, L. J., Evans, C. J., Lennon, D. J., & Bouret, J. C. 2003, *ApJ*, 588, 1039
- Hillier, D. J., & Miller, D. L. 1998, *ApJ*, 496, 407
- . 1999, *ApJ*, 519, 354
- Hora, J. L., et al. 2008, *AJ*, 135, 726
- Howarth, I. D. 1983, *MNRAS*, 203, 301
- Hua, C. T., & Kwok, S. 1999, *A&AS*, 138, 275

- Hügelmeier, S. D., Dreizler, S., Werner, K., Krzesinski, J., Nitta, A., & Kleinman, S. J. 2007, in *Astronomical Society of the Pacific Conference Series*, Vol. 372, 15th European Workshop on White Dwarfs, ed. R. Napiwotzki & M. R. Burleigh, 249
- Iben, Jr., I. 1995, *Phys. Rep.*, 250, 2
- Iben, Jr., I., Kaler, J. B., Truran, J. W., & Renzini, A. 1983, *ApJ*, 264, 605
- Indebetouw, R., et al. 2005, *ApJ*, 619, 931
- Isobe, T., Feigelson, E. D., Akritas, M. G., & Babu, G. J. 1990, *ApJ*, 364, 104
- Jacoby, G. H., & Ford, H. C. 1983, *ApJ*, 266, 298
- Jacoby, G. H., et al. 2010, *PASA*, 27, 156
- Jeffery, C. S., Heber, U., Hill, P. W., Dreizler, S., Drilling, J. S., Lawson, W. A., Leuenhagen, U., & Werner, K. 1996, in *Astronomical Society of the Pacific Conference Series*, Vol. 96, Hydrogen Deficient Stars, ed. C. S. Jeffery & U. Heber, 471
- Kaler, J. B. 1997, *Stars and their Spectra*, ed. Kaler, J. B.
- Kaler, J. B., Shaw, R. A., & Kwitter, K. B. 1990, *ApJ*, 359, 392
- Karakas, A. I., Lattanzio, J. C., & Pols, O. R. 2002, *PASA*, 19, 515
- Kastner, J. H., Weintraub, D. A., Gatley, I., Merrill, K. M., & Probst, R. G. 1996, *ApJ*, 462, 777
- Kawamura, J., & Masson, C. 1996, *ApJ*, 461, 282
- Kerber, F., Mignani, R. P., Guglielmetti, F., & Wicenec, A. 2003, *A&A*, 408, 1029
- Kimeswenger, S., Zijlstra, A. A., van Hoof, P. A. M., Hajduk, M., Herwig, F., Lechner, M. F. M., Eyres, S. P. S., & van de Steene, G. C. 2008, in *Astronomical Society of*

- the Pacific Conference Series, Vol. 391, Hydrogen-Deficient Stars, ed. A. Werner & T. Rauch, 177
- Kingsburgh, R. L., & Barlow, M. J. 1994, *MNRAS*, 271, 257
- Kingsburgh, R. L., Barlow, M. J., & Storey, P. J. 1995, *A&A*, 295, 75
- Koenigsberger, G., & Moreno, E. 2008, in *Revista Mexicana de Astronomia y Astrofisica*, vol. 27, Vol. 33, *Revista Mexicana de Astronomia y Astrofisica Conference Series*, 108–112
- Koesterke, L. 2001, *Ap&SS*, 275, 41
- Koesterke, L., & Hamann, W. 1995, *A&A*, 299, 503
- Koesterke, L., & Hamann, W. 1997a, in *IAU Symposium*, Vol. 180, *Planetary Nebulae*, ed. H. J. Habing & H. J. G. L. M. Lamers, 114
- . 1997b, *A&A*, 320, 91
- Kogure, T., Kobayashi, Y., Sasaki, T., Sakka, K., Miyajima, K., & Nakano, M. 1982, *Contribution from the Department of Astronomy, University of Kyoto*, 133
- Kohoutek, L. 2001, *A&A*, 378, 843
- . 2002, *Astronomische Nachrichten*, 323, 57
- Köppen, J., Acker, A., & Stenholm, B. 1991, *A&A*, 248, 197
- Kurosawa, R., Hillier, D. J., & Schulte-Ladbeck, R. E. 1999, *AJ*, 118, 539
- Lamers, H. J. G. L. M., Maeder, A., Schmutz, W., & Cassinelli, J. P. 1991, *ApJ*, 368, 538
- Lamers, H. J. G. L. M., & Nugis, T. 2002, *A&A*, 395, L1

- Langer, N. 1990, in *Astronomical Society of the Pacific Conference Series*, Vol. 7, *Properties of Hot Luminous Stars*, ed. C. D. Garmany, 328–339
- Langer, N., Hamann, W., Lennon, M., Najarro, F., Pauldrach, A. W. A., & Puls, J. 1994, *A&A*, 290, 819
- Lasker, B. M., et al. 2008, *AJ*, 136, 735
- Lau, H. H. B., De Marco, O., & Liu, X. 2010, *Mem. Soc. Astron. Ital.*, 81, 1045
- Lau, H. H. B., Stancliffe, R. J., & Tout, C. A. 2009, *MNRAS*, 396, 1046
- Lawrence, A., et al. 2007, *MNRAS*, 379, 1599
- Leuenhagen, U., & Hamann, W. 1994, *A&A*, 283, 567
- . 1998, *A&A*, 330, 265
- Leuenhagen, U., Hamann, W., & Jeffery, C. S. 1996, *A&A*, 312, 167
- Li, J., Harrington, J. P., & Borkowski, K. J. 2002, *AJ*, 123, 2676
- MacFadyen, A. I., & Woosley, S. E. 1999, *ApJ*, 524, 262
- Maciel, W. J. 1989, in *IAU Symposium*, Vol. 131, *Planetary Nebulae*, ed. S. Torres-Peimbert, 213
- Madsen, G. J., Frew, D. J., Parker, Q. A., Reynolds, R. J., & Haffner, L. M. 2006, in *IAU Symposium*, Vol. 234, *Planetary Nebulae in our Galaxy and Beyond*, ed. M. J. Barlow & R. H. Méndez, 455–456
- Maeder, A. 1989, in *Astrophysics and Space Science Library*, Vol. 157, *IAU Colloq. 113: Physics of Luminous Blue Variables*, ed. K. Davidson, A. F. J. Moffat, & H. J. G. L. M. Lamers, 15–23
- Magakian, T. Y. 2003, *A&A*, 399, 141

- Malesani, D., et al. 2004, *ApJ*, 609, L5
- Mallik, D. C. V., & Peimbert, M. 1988, *RMxAA*, 16, 111
- Malmquist, K. G. 1924, *MeLuAO*, 2, 64
- Marchenko, S. V., et al. 2004, *MNRAS*, 353, 153
- Marcolino, W. L. F., & de Araújo, F. X. 2003, *AJ*, 126, 887
- Marcolino, W. L. F., de Araújo, F. X., Junior, H. B. M., & Duarte, E. S. 2007a, *AJ*, 134, 1380
- Marcolino, W. L. F., Hillier, D. J., de Araujo, F. X., & Pereira, C. B. 2007b, *ApJ*, 654, 1068
- Martin, P. G. 1999, in *Astronomical Society of the Pacific Conference Series*, Vol. 168, *New Perspectives on the Interstellar Medium*, ed. A. R. Taylor, T. L. Landecker, & G. Joncas, 108
- Massey, P. 1980, *ApJ*, 236, 526
- . 2003, *ARA&A*, 41, 15
- Massey, P., & Conti, P. S. 1981, *ApJ*, 244, 173
- Mazzali, P. A., et al. 2003, *ApJ*, 599, L95
- McCullough, P. R., Bender, C., Gaustad, J. E., Rosing, W., & Van Buren, D. 2001, *AJ*, 121, 1578
- McGregor, P. J., Conroy, P., Bloxham, G., & van Harmelen, J. 1999, *PASA*, 16, 273
- McGregor, P. J., et al. 2003, in *Society of Photo-Optical Instrumentation Engineers (SPIE) Conference Series*, Vol. 4841, *Society of Photo-Optical Instrumentation Engineers (SPIE) Conference Series*, ed. M. Iye & A. F. M. Moorwood, 1581–1591

- McKibben Nail, V., & Shapley, H. 1955, *Proceedings of the National Academy of Science*, 41, 685
- Meatheringham, S. J., Wood, P. R., & Faulkner, D. J. 1988, *ApJ*, 334, 862
- Medina, S., & Peña, M. 2002, in *Revista Mexicana de Astronomia y Astrofisica Conference Series*, Vol. 12, *Revista Mexicana de Astronomia y Astrofisica Conference Series*, ed. W. J. Henney, J. Franco, & M. Martos, 169–169
- Medina, S., Peña, M., Morisset, C., & Stasińska, G. 2006, *RMxAA*, 42, 53
- Mellema, G. 2004, *A&A*, 416, 623
- Mendez, R. H. 1991, in *IAU Symposium*, Vol. 145, *Evolution of Stars: the Photospheric Abundance Connection*, ed. G. Michaud & A. V. Tutukov, 375
- Mendez, R. H., Herrero, A., & Manchado, A. 1990, *A&A*, 229, 152
- Mendez, R. H., Kudritzki, R. P., Gruschinske, J., & Simon, K. P. 1981, *A&A*, 101, 323
- Mendez, R. H., Kudritzki, R. P., Herrero, A., Husfeld, D., & Groth, H. G. 1988, *A&A*, 190, 113
- Meynet, G., & Maeder, A. 2005, *A&A*, 429, 581
- Miller Bertolami, M. M., & Althaus, L. G. 2006, *A&A*, 454, 845
- . 2007, *MNRAS*, 380, 763
- Miller Bertolami, M. M., Althaus, L. G., Serenelli, A. M., & Panei, J. A. 2006, *A&A*, 449, 313
- Miszalski, B., Acker, A., Moffat, A. F. J., Parker, Q. A., & Udalski, A. 2009a, *A&A*, 496, 813
- Miszalski, B., Acker, A., Parker, Q. A., & Moffat, A. F. J. 2009b, *A&A*, 505, 249

- Miszalski, B., Parker, Q. A., Acker, A., Birkby, J. L., Frew, D. J., & Kovacevic, A. 2008, *MNRAS*, 384, 525
- Moffat, A. F. J., Drissen, L., & Robert, C. 1989, in *Astrophysics and Space Science Library*, Vol. 157, IAU Colloq. 113: *Physics of Luminous Blue Variables*, ed. K. Davidson, A. F. J. Moffat, & H. J. G. L. M. Lamers, 229–237
- Moffat, A. F. J., & Robert, C. 1994, *ApJ*, 421, 310
- Monk, D. J., Barlow, M. J., & Clegg, R. E. S. 1988, *MNRAS*, 234, 583
- Monteiro, H., Schwarz, H. E., Gruenwald, R., & Heathcote, S. 2004, *ApJ*, 609, 194
- Montez, Jr., R., Kastner, J. H., De Marco, O., & Soker, N. 2005, *ApJ*, 635, 381
- Morgan, D. H. 1984, *MNRAS*, 208, 633
- Morgan, D. H., Parker, Q. A., & Cohen, M. 2003, *MNRAS*, 346, 719
- Nakamura, T., Mazzali, P. A., Nomoto, K., & Iwamoto, K. 2001, *ApJ*, 550, 991
- Norci, L., Polcaro, V. F., Rossi, C., & Viotti, R. 1998, *Irish Astronomical Journal*, 25, 43
- Oliver, R. J., Mashedier, M. R. W., & Thaddeus, P. 1996, *A&A*, 315, 578
- Osterbrock, D. E., & Ferland, G. J. 2006, *Astrophysics of gaseous nebulae and active galactic nuclei*, ed. Osterbrock, D. E. & Ferland, G. J.
- Owocki, S. P., Cranmer, S. R., & Gayley, K. G. 1996, *ApJ*, 472, L115+
- Page, T. 1942, *ApJ*, 96, 78
- Palen, S., Balick, B., Hajian, A. R., Terzian, Y., Bond, H. E., & Panagia, N. 2002, *AJ*, 123, 2666

- Parker, J. W., Clayton, G. C., Winge, C., & Conti, P. S. 1993, *ApJ*, 409, 770
- Parker, Q. A., & Frew, D. J. 2011, in *Asymmetric Planetary Nebulae 5 Conference*
- Parker, Q. A., & Malin, D. 1999, *PASA*, 16, 288
- Parker, Q. A., & Morgan, D. H. 2003, *MNRAS*, 341, 961
- Parker, Q. A., Phillipps, S., & Morgan, D. H. 1999, in *Astronomical Society of the Pacific Conference Series, Vol. 168, New Perspectives on the Interstellar Medium*, ed. A. R. Taylor, T. L. Landecker, & G. Joncas, 126
- Parker, Q. A., Watson, F. G., & Miziarski, S. 1998, in *Astronomical Society of the Pacific Conference Series, Vol. 152, Fiber Optics in Astronomy III*, ed. S. Arribas, E. Mediavilla, & F. Watson, 80
- Parker, Q. A., et al. 2005, *MNRAS*, 362, 689
- . 2006, *MNRAS*, 373, 79
- Parthasarathy, M., Acker, A., & Stenholm, B. 1998, *A&A*, 329, L9
- Peña, M. 1995, in *Revista Mexicana de Astronomia y Astrofisica Conference Series, Vol. 3, Revista Mexicana de Astronomia y Astrofisica Conference Series*, ed. M. Peña & S. Kurtz, 215
- Peña, M. 2002, in *Revista Mexicana de Astronomia y Astrofisica, vol. 27, Vol. 12, Revista Mexicana de Astronomia y Astrofisica Conference Series*, ed. W. J. Henney, J. Franco, & M. Martos, 148–149
- Peña, M., Hamann, W., Koesterke, L., Maza, J., Mendez, R. H., Peimbert, M., Ruiz, M. T., & Torres-Peimbert, S. 1997a, *ApJ*, 491, 233
- . 1997b, *ApJ*, 491, 233

- Peña, M., Medina, S., & Stasińska, G. 2003a, in *Revista Mexicana de Astronomía y Astrofísica Conference Series*, Vol. 18, *Revista Mexicana de Astronomía y Astrofísica Conference Series*, ed. M. Reyes-Ruiz & E. Vázquez-Semadeni, 84–89
- Peña, M., Medina, S., & Stasińska, G. 2003b, in *Revista Mexicana de Astronomía y Astrofísica Conference Series*, Vol. 15, *Revista Mexicana de Astronomía y Astrofísica Conference Series*, ed. J. Arthur & W. J. Henney, 38–40
- Peña, M., Peimbert, A., Hamann, W., Ruiz, M. T., & Peimbert, M. 2004, in *Astronomical Society of the Pacific Conference Series*, Vol. 313, *Asymmetrical Planetary Nebulae III: Winds, Structure and the Thunderbird*, ed. M. Meixner, J. H. Kastner, B. Balick, & N. Soker, 131
- Peña, M., Peimbert, M., Torres-Peimbert, S., Ruiz, M. T., & Maza, J. 1995, *ApJ*, 441, 343
- Peña, M., & Ruiz, M. T. 1988, *RMxAA*, 16, 55
- Peña, M., Ruiz, M. T., & Torres-Peimbert, S. 1997c, *A&A*, 324, 674
- Peña, M., Stasińska, G., Esteban, C., Koesterke, L., Medina, S., & Kingsburgh, R. 1998, *A&A*, 337, 866
- Peña, M., Stasińska, G., & Medina, S. 2001, *A&A*, 367, 983
- Peimbert, M. 1978, in *IAU Symposium*, Vol. 76, *Planetary Nebulae*, ed. Y. Terzian, 215–223
- Peimbert, M., & Serrano, A. 1980, *RMxAA*, 5, 9
- Peimbert, M., & Torres-Peimbert, S. 1983, in *IAU Symposium*, Vol. 103, *Planetary Nebulae*, ed. D. R. Flower, 233–241
- Peimbert, M., & Torres-Peimbert, S. 1987, *RMxAA*, 14, 540

- Pereira, C. B., & Machado, M. 2003, *A&A*, 407, 311
- Perek, L. 1960, *Bulletin of the Astronomical Institutes of Czechoslovakia*, 11, 256
- Perinotto, M. 2007, *Mem. Soc. Astron. Ital.*, 78, 530
- Phillipps, S., & Parker, Q. A. 1993, *MNRAS*, 265, 385
- Phillips, J. P. 2001, *MNRAS*, 326, 1041
- Phillips, J. P., & Ramos-Larios, G. 2008, *MNRAS*, 383, 1029
- Pierce, M. J., Frew, D. J., Parker, Q. A., & Köppen, J. 2004, *PASA*, 21, 334
- Pollacco, D. L., & Bell, S. A. 1993, *MNRAS*, 262, 377
- . 1994, *MNRAS*, 267, 452
- Pottasch, S. R. 1996, *A&A*, 307, 561
- Preite-Martinez, A. 1988, *A&AS*, 76, 317
- Quirion, P., Fontaine, G., & Brassard, P. 2007, *ApJS*, 171, 219
- Reach, W. T., et al. 2006, *AJ*, 131, 1479
- Reay, N. K., Atherton, P. D., & Taylor, K. 1983, in *IAU Symposium, Vol. 103, Planetary Nebulae*, ed. D. R. Flower, 508
- Reed, D. S., Balick, B., Hajian, A. R., Klayton, T. L., Giovanardi, S., Casertano, S., Panagia, N., & Terzian, Y. 1999, *AJ*, 118, 2430
- Reid, W. A., & Parker, Q. A. 2010, *PASA*, 27, 187
- Reynolds, R. J., Tufte, S. L., Haffner, L. M., Jaehnig, K., & Percival, J. W. 1998, *PASA*, 15, 14

- Ringat, E., Friederich, F., Rauch, T., Werner, K., & Kruk, J. W. 2011, in *Asymmetric Planetary Nebulae 5 Conference*
- Robinson, G. J., Reay, N. K., & Atherton, P. D. 1982, *MNRAS*, 199, 649
- Rodgers, A. W., Campbell, C. T., & Whiteoak, J. B. 1960, *MNRAS*, 121, 103
- Rodgers, A. W., Conroy, P., & Bloxham, G. 1988, *PASP*, 100, 626
- Rosseland, S. 1938, *MNRAS*, 98, 301
- Russeil, D. 1997, *A&A*, 319, 788
- Russeil, D., Georgelin, Y. M., Amram, P., Georgelin, Y. P., Laval, A., & Marcelin, M. 1998, *PASA*, 15, 9
- Sabbadin, F. 1984, *A&AS*, 58, 273
- Sabogal, B. E., Mennickent, R. E., Pietrzyński, G., García, J. A., Gieren, W., & Kolaczowski, Z. 2008, *A&A*, 478, 659
- Salpeter, E. E. 1955, *ApJ*, 121, 161
- Sanduleak, N., MacConnell, D. J., & Philip, A. G. D. 1978, *PASP*, 90, 621
- Saunders, W., et al. 2004, in *Presented at the Society of Photo-Optical Instrumentation Engineers (SPIE) Conference, Vol. 5492, Society of Photo-Optical Instrumentation Engineers (SPIE) Conference Series*, ed. A. F. M. Moorwood & M. Iye, 389–400
- Schlegel, D. J., Finkbeiner, D. P., & Davis, M. 1998, *ApJ*, 500, 525
- Schmutz, W., Hamann, W., & Wessolowski, U. 1989, *A&A*, 210, 236
- Schoenberner, D. 1979, *A&A*, 79, 108
- Schönberner, D., Jacob, R., & Steffen, M. 2005, *A&A*, 441, 573

- Seaton, M. J. 1954, MNRAS, 114, 154
- Sharp, R., & The Aaomega+Spiral Team. 2006a, Anglo-Australian Observatory Epping Newsletter, 110, 24
- . 2006b, Anglo-Australian Observatory Epping Newsletter, 110, 24
- Shaw, R. A., & Kaler, J. B. 1989, ApJS, 69, 495
- Sion, E. M., Holberg, J. B., Oswalt, T. D., McCook, G. P., & Wasatonic, R. 2009, AJ, 138, 1681
- Skutskie, M. F., et al. 2006, AJ, 131, 1163
- Smith, L. F., & Aller, L. H. 1969, ApJ, 157, 1245
- Smith, L. F., & Maeder, A. 1991, A&A, 241, 77
- Smith, L. J., Crowther, P. A., & Prinja, R. K. 1994, A&A, 281, 833
- Smith, N., et al. 2007, ApJ, 666, 1116
- Soker, N. 1997, ApJS, 112, 487
- St.-Louis, N., & Moffat, A. F. J., eds. 2007, Astronomical Society of the Pacific Conference Series, Vol. 367, Massive Stars in Interactive Binaries
- Stancliffe, R. J. 2010, MNRAS, 403, 505
- Stanghellini, L. 2000, Ap&SS, 272, 181
- Stanghellini, L., Shaw, R. A., Balick, B., Mutchler, M., Blades, J. C., & Villaver, E. 2003, ApJ, 596, 997
- Stanghellini, L., Shaw, R. A., & Villaver, E. 2008, ApJ, 689, 194
- Stanghellini, L., Villaver, E., Manchado, A., & Guerrero, M. A. 2002, ApJ, 576, 285

- Steffen, W., López, J. A., & Lim, A. J. 2002, in *Revista Mexicana de Astronomía y Astrofísica*, vol. 27, Vol. 13, *Revista Mexicana de Astronomía y Astrofísica Conference Series*, ed. W. J. Henney, W. Steffen, L. Binette, & A. Raga, 150–154
- Steiner, J. E., & Diaz, M. P. 1998, *PASP*, 110, 276
- Sterling, N. C., & Dinerstein, H. L. 2008, *ApJS*, 174, 158
- Storey, P. J., & Zeippen, C. J. 2000, *MNRAS*, 312, 813
- Stothers, R. B., & Chin, C. 1995, *ApJ*, 451, L61+
- Suárez, O., García-Lario, P., Manchado, A., Manteiga, M., Ulla, A., & Pottasch, S. R. 2006, *A&A*, 458, 173
- Todt, H., Gräfener, G., & Hamann, W. 2006, in *IAU Symposium*, Vol. 234, *Planetary Nebulae in our Galaxy and Beyond*, ed. M. J. Barlow & R. H. Méndez, 127–130
- Todt, H., Peña, M., Hamann, W., & Gräfener, G. 2008, in *Astronomical Society of the Pacific Conference Series*, Vol. 391, *Hydrogen-Deficient Stars*, ed. A. Werner & T. Rauch, 95
- Todt, H., Peña, M., Hamann, W., & Gräfener, G. 2010, *A&A*, 515, A83+
- Torres, A. V., Conti, P. S., & Massey, P. 1986, *ApJ*, 300, 379
- Torres-Peimbert, S., Peimbert, M., Ruiz, M. T., & Peña, M. 1993, in *IAU Symposium*, Vol. 155, *Planetary Nebulae*, ed. R. Weinberger & A. Acker, 584
- Tylenda, R. 1989, in *IAU Symposium*, Vol. 131, *Planetary Nebulae*, ed. S. Torres-Peimbert, 531–537
- Tylenda, R. 1996, in *Astronomical Society of the Pacific Conference Series*, Vol. 96, *Hydrogen Deficient Stars*, ed. C. S. Jeffery & U. Heber, 101

- Tylenda, R., Acker, A., & Stenholm, B. 1993, *A&AS*, 102, 595
- Tylenda, R., & Stasińska, G. 1989, in *IAU Symposium*, Vol. 131, *Planetary Nebulae*, ed. S. Torres-Peimbert, 542
- Tylenda, R., & Stasińska, G. 1994, *A&A*, 288, 897
- Unglaub, K., & Bues, I. 2000, *A&A*, 359, 1042
- Vacca, W. D., Garmany, C. D., & Shull, J. M. 1996, *ApJ*, 460, 914
- van der Hucht, K. A. 2001, *NewAR*, 45, 135
- . 2006, *A&A*, 458, 453
- van der Hucht, K. A., Conti, P. S., Lundstrom, I., & Stenholm, B. 1981, *Space Sci. Rev.*, 28, 227
- van der Hucht, K. A., Hidayat, B., Admiranto, A. G., Supelli, K. R., & Doom, C. 1988, *A&A*, 199, 217
- van Dokkum, P. G. 2001, *PASP*, 113, 1420
- Vassiliadis, E., & Wood, P. R. 1993, *ApJ*, 413, 641
- Villaver, E., Stanghellini, L., & Shaw, R. A. 2003, *ApJ*, 597, 298
- . 2007, *ApJ*, 656, 831
- Vink, J. S., & de Koter, A. 2005, *A&A*, 442, 587
- von Zeipel, H. 1924, *MNRAS*, 84, 665
- Vreux, J. M., Dennefeld, M., & Andrillat, Y. 1983, *A&AS*, 54, 437
- Wachter, S., Mauerhan, J. C., Van Dyk, S. D., Hoard, D. W., Kafka, S., & Morris, P. W. 2010, *AJ*, 139, 2330

- Wackerling, L. R. 1970, *MmRAS*, 73, 153
- Walborn, N. R. 1971, *ApJS*, 23, 257
- . 1982, *ApJ*, 256, 452
- Walsh, J. R., Dudziak, G., Minniti, D., & Zijlstra, A. A. 1997, *ApJ*, 487, 651
- Wang, Q. 1991, *MNRAS*, 252, 47P
- Webster, B. L. 1975, *MNRAS*, 173, 437
- Weedman, D. W. 1968, *PASP*, 80, 314
- Weidmann, W. A., & Gamen, R. 2011, *A&A*, 526, A6+
- Weinberger, R. 1989, *A&AS*, 78, 301
- Werner, K. 1992, in *Lecture Notes in Physics*, Berlin Springer Verlag, Vol. 401, *The Atmospheres of Early-Type Stars*, ed. U. Heber & C. S. Jeffery, 273
- Werner, K., Dreizler, S., Heber, U., Kappelman, N., Kruk, J., Rauch, T., & Wolff, B. 1997, in *Reviews in Modern Astronomy*, Vol. 10, *Reviews in Modern Astronomy*, ed. R. E. Schielicke, 219–252
- Werner, K., Hamann, W., Heber, U., Napiwotzki, R., Rauch, T., & Wessolowski, U. 1992, *A&A*, 259, L69
- Werner, K., & Herwig, F. 2006, *PASP*, 118, 183
- Werner, K., Rauch, T., Reiff, E., & Kruk, J. W. 2009, *Ap&SS*, 320, 159
- Wesson, R., Barlow, M. J., Liu, X., Storey, P. J., Ercolano, B., & De Marco, O. 2008, *MNRAS*, 383, 1639
- Wesson, R., Liu, X., & Barlow, M. J. 2003, *MNRAS*, 340, 253

- Westerlund, B. E., & Smith, L. F. 1964, MNRAS, 127, 449
- Wolf, C. J. E., & Rayet, G. 1867, Comptes Rendus Acad. Sci., 65, 292
- Woosley, S. E., & Bloom, J. S. 2006, ARA&A, 44, 507
- Wray, J. D. 1966, PhD thesis, Northwestern University.
- Yasuda, N., Fukugita, M., & Schneider, D. P. 2007, AJ, 134, 698
- Zacharias, N., Monet, D. G., Levine, S. E., Urban, S. E., Gaume, R., & Wycoff, G. L. 2004, in Bulletin of the American Astronomical Society, Vol. 36, American Astronomical Society Meeting Abstracts, 1418
- Zhang, C. Y., & Kwok, S. 1993, ApJS, 88, 137
- Zijlstra, A. A., Gesicki, K., Walsh, J. R., Péquignot, D., van Hoof, P. A. M., & Minniti, D. 2006, MNRAS, 369, 875
- Zijlstra, A. A., & Pottasch, S. R. 1991, A&A, 243, 478
- Zuckerman, B., & Aller, L. H. 1986, ApJ, 301, 772
- Zuckerman, B., & Gatley, I. 1988, ApJ, 324, 501